A numerical study of the effect of aortic wall compliance and blood flow through the ascending aorta

Helen Lorna Morrissey

Thesis presented in fulfillment
blah blah blah for the Degree of BSc in Mechanical Engineering

Department of Mechanical Engineering
University of Cape Town

November 1, 2006

Abstract

The ascending aorta is located at the outflow tract of the heart and its function is to supply the body with oxygenated blood from the lungs. Any damage to the ascending aorta as a result of age or disease can have severe effects on the entire body.
A computational study of both the artery wall tissue and the blood flow in the aorta and the coupling of these two systems, to find the effects on aortic compliance is described in this report. The investigation involved one fluid model (analysed with CFD) coupled with three models of a healthy aorta, and one model of a diseased aorta (analysed with FEM). Various programmes were created in Matlab to couple the solid and fluid systems.

The aorta was modelled as a straight cylinder and thus the solid and fluid models were assumed as axi-symmetric. Blood was modelled as Newtonian, with constant density and viscosity values. A steady blood flow model was defined, and the flow was modelled as laminar.
Arteries are comprised of three layers, the intima, media and adventitia, however the intimal layer is very thin in a healthy artery and its effect was assumed negligible in the healthy artery models. Constitutive equations were developed for the artery walls, which described a linear elastic, transversely isotropic material. A bottom-up engineering approach was taken and the aorta was first modelled as isotropic, consisting of only one averaged layer, then as isotropic, consisting of an adventitial layer and a medial layer, and finally as orthotropic, consisting of the adventitial and medial layers. The thickening of the intima was then induced in the models to approximate an artery affected by arteriosclerosis.

The results showed an increase in aortic compliance from the initial model to the final model. It was also found that the effect of blood flow in the coupled simulations increased the compliance of the ascending aorta.
It was concluded that as the values of compliance were within the measured range under physiological conditions the coupled investigation was successful. However various improvements can be made to the models, in terms of the material models, pulsatility of the blood flow and a three-dimensional model of the aorta.

Declaration

1 I know that plagiarism is wrong. Plagiarism is to use of another's work and pretend that it is one's own.
2 I have used the Vancouver convention for citation and referencing. Each significant contribution to, and quotation in, this report from the works of other
people has been attributed, and has been cited and referenced.
3 This report is my own work.
4 I have not allowed, and will not allow anyone to copy my work with the intention of passing it off as his or her own work.

Signature .....
Helen Lorna Morrissey

Acknowledgements

I would like to thank Dr C.J. Meyer for his help and concern during the course of this project; in spite of his broken leg he has done everything he can to make his students as comfortable as possible with their theses. Thank you to Professor B.D. Reddy for his calm and reassuring assistance in this project and for knowing everything that I don't. I would also like to thank him and Dr T. Franz for proposing such an interesting topic and allowing me to tackle it.

Thanks must also go to Helena vd Merwe for her willingness to help me with any ABAQUS® problems that I encountered, and for making her way up to Upper Campus just for this purpose.

I would like to thank everyone at BISRU for being so willing to help me with ABAQUS® , especially to Pierre le Roux for his general support and Victor Balden for solving my three week problems in the space of two hours.

The help received from the post-graduates in CERECAM has been indispensable in this project, thank heavens for you guys. Thank you for teaching me almost everything I know about computers; no more editing documents with black fineliner. So thank you Andrew, Amy, Darnell, Dwain, JP, Kevin and Vani, you may have saved my life a few times.

My undergraduate colleagues, thanks so much, you have been both entertaining and supportive. A special thank you goes to Marlan Perumal, what would I have done without you?

Finally, thank you to my family, friends and Beetchis, for their endless encouragement and support, you are my gifts from God.

Nomenclature

Symbols

C_d	Compliance
D_d	Diameter (m)
E	Elastic modulus (Pa)
f	Frequency (Hz)
k	Stiffness $(N.m^{-1})$
L_{init}	Initial length (m)
ν	Poissons ratio
p	Pressure (Pa)
r	Radius (m)
Ψ	Strain energy $(m^2.s^{-2})$
σ	Stress (Pa)
u	Displacement (m)
v	Velocity $(m.s^{-1})$

Greek Symbols

γ	Shear strain $(-)$
θ	Rotation (rad)

ρ Density ($kg.m^{-3}$)

τ Shear stress (Pa)

μ Viscosity ($kg.m^{-1}s^{-1}$)

Acronyms

CFD Computational Fluid Dynamics

FEM Finite Element Method

UDF User Defined Function

Glossary

Adventitia	The outermost layer of the artery
Anteriorly	Towards the front of the body
Arterial system	The system of blood vessels transporting oxygenated blood from the heart to the body
Arteriosclerosis	An unhealthy condition when there is a thickening and resulting stiffening of the artery wall
Atherosclerosis	An unhealthy condition when there is a build up of compounds such as cholestorol inside the artery, which negatively affects its compliant properties
Bifurcation	The branching of a single artery into two or more separate arteries
Compliance/Distensibility	A measure of the change in diameter with pressure applied
Constitutive equations	Mathematical equations completely describing the material behaviour of a substance

Diastole	The condition when the heart dilates, creating the lower blood pressure value
Flat velocity profile	A constant velocity at all parallel points at the flow inlet
Hyperelasticity	Non-linear elasticity
Intima	The innermost layer of the artery
Isotropic	A material with the same elastic properties in all directions
Media	The middle layer of the artery
Orthotropic/Transversely isotropic	A material with different elastic properties in two, orthogonal directions
Reynolds number	Ratio of inertial forces to viscous forces
Rheology	The study of non-Newtonian fluids
Systole	The condition when the heart contracts, creating the upper blood pressure value
Venous system	The system of blood vessels returning deoxygenated blood from the body to the heart

Viscoelasticity	Material properties resembling those of both a solid and a fluid

Contents

List of Figures

List of Tables

Chapter 1

Introduction

1.1 Motivation

The study of biomechanics (mechanics applied to biology) allows a deeper understanding of living systems. Most biomechanical studies concentrate on physiological and medical applications. The study of biology from a mechanical point of view enables an understanding of the body under normal conditions, prediction of the effects of any changes and the provision of prevention and intervention in case of adverse changes [6].

As the first section of the aorta, the ascending aorta plays a vital role in the human body, that of transporting oxygenated blood from the lungs to all other organs and limbs, including the heart itself. If blood supply to a muscle is cut off for more than a few minutes, the muscle cells may experience permanent injury and, especially in the case of the heart muscle, damage may induce severe disabilities or even death [2].

Prevention and correction of any form of degeneration of the ascending aorta is paramount, with bypass surgery and stenting being typical methods of correction and prevention of failure. For the diagnosis of any ill conditions and for the design and improvement of any prosthesis to be advantageous, it is important that there is detailed knowledge and understanding of the stress and strain conditions in the aorta [7], [8]. Detailed information about the stresses and strains in the aorta under physiological conditions can be deduced via computational methods, in particular the use of the finite element and finite volume methods in solving equations of solid deformation and fluid flow approximately. The coupled simulation of blood flow and wall deformation in the ascending aorta further deepens the understanding of the interaction of the character-

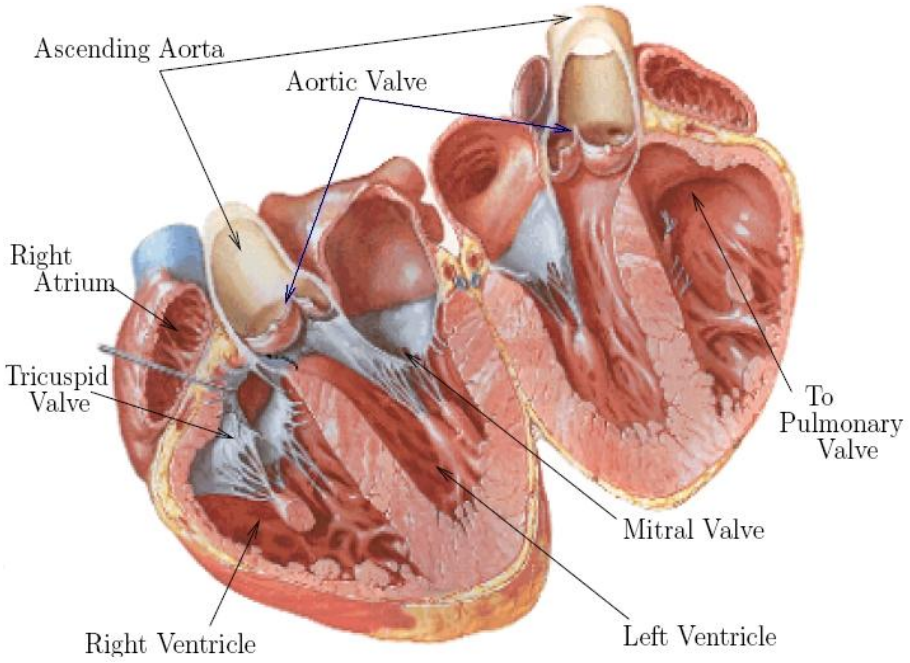

Figure 1.1: Diagram showing the valves and chambers of the heart, and the location of the ascending aorta (modified from [1])

istics of the aortic system.
The resolution of the flow field and the analysis of the deformations resulting from the pressure induced by the flow, can provide useful information but require the communication of these variables.

One of the main advantages of computational investigations into biological systems, as a complement to experimental and clinical methods, lies in the opportunity to perform virtual experiments and simulate situations on a system that could be inconvenient, dangerous, complicated or even impossible in a practical form.

The purpose of this investigation is to create a numerical approximation to t he coupled problem of blood flow through, and deformation of the human ascending aorta. This allows the discovery of the artery wall stresses and strains as well as blood flow and pressure as a result of the interaction between blood flow and the compliant action of the artery wall.
The location of the ascending aorta with the heart's chambers and valves is shown in Figure 1.1.

1.2 Theoretical Approach

The potential value of a realistic coupled simulation of the blood flow and wall deformation in the ascending aorta lies in the reliability of the results. Thus the desired model includes as many parameters as possible to closely resemble physiological conditions.

At the outset of this investigation it was expected that the coupling software MpCCI® would be used to communicate the relevant information between the solid analysis software and the computational fluid dynamics software. As this communication was to be dealt with via sophisticated software the original model was to be a three dimensional model, which took into account the transient nature of (pulsatile) blood flow.
It was soon established, from a documented analysis performed using MpCCI® [8] however, that simulations for pulsatile flow modelling in the aorta would be extremely time consuming and unlikely to be feasible within the time constraints of the investigation. Thus the pulsatile flow aspect of the investigation was discarded.
After much time and effort from all concerned with the various licensing and installation aspects of MpCCI® , it became clear that there was some form of error preventing the software from being effective immediately.
Also, the nature of MpCCI® is such that a considerable amount of time was needed to fully understand the programme. Therefore, due to the time constraints it was decided that the MpCCI® would not be employed in this thesis.
As a result of this the scope of the investigation was altered to include the programming of an effective interface between the FEM and CFD packages to reduce manual transfer as far as possible. To simplify the coding, it was decided that the ascending aorta would be modelled axisymmetrically and that the coupling would consist of a series of static steps in the independant FEM and CFD models, which are updated with the field defined in the preceding job.

1.3 Objectives

The main objectives of this thesis are to:

- build on basic knowledge of the solid analysis package ABAQUS® and use it to develop a finite element model of the human ascending aorta
- become familiar with the CFD pre-processor GAMBIT® and use it to create a suitable flow domain

- become familiar with the CFD solver package FLUENT® and use it to develop a model of blood flow in the human ascending aorta
- investigate and understand the format of the text based input and output files of both ABAQUS® and FLUENT® so as to create a programme, using the mathematical programming language Matlab, to import and export data to and from ABAQUS® and FLUENT® to create a coupling between the solid and fluid problems
- create in the above manner models characterising a healthy, young ascending aorta as well as an aged and/or diseased ascending aorta
- provide a comparison between the different models used, to illustrate the effects of various human body phenomena existing in the ascending aorta as well as the effects of degenerative conditions on the artery

1.4 Plan of Development

The report starts with a review of existing numerical models of arterial systems used in the course of this investigation. This is followed by detailed descriptions of the various models analysed as well as relevant theoretical information on the biological system. The results of these analyses are then presented and discussed. Conclusions are then drawn based on these results and finally recommendations are given for further analyses which may be carried out.

Chapter 2

Literature Review

Information on the methods used and previous models in this field are included in this chapter. A brief overview of the circulatory system and the ascending aorta is also provided here. Theory specific to the individual modelling sections is not included here, but is detailed in the corresponding chapters.

2.1 Finite Element Analysis

Finite element analysis is a computational method used for solving the governing equations of mechanical and other systems approximately. This method can be applied to stress analysis to calculate stress and displacement fields. The finite element method involves dividing a structure into finite elements, formed of a number of nodes, and interpolating the field quantity (i.e. stress or displacement) between these nodes [9].
The set of simultaneous equations that is generated can then be solved to find values for the field quantity as desired. The problem set up requires the definition of geometry, material properties, loading conditions and boundary constraints [9].
In stress analysis the simultaneous equations solve the equilibrium conditions.
Three steps are involved in this process as follows:

1. Pre-processing
   A structural definition for the problem is given in this step and a suitable mesh is created. Boundary conditions are defined, allowing or constraining certain displacements and rotations. The loading conditions are also defined in this step.

2. Solver
   The matrix of simultaneous equations is solved computationally in this step to

satisfy solid equilibrium.

3. Post-processing
   The results may be analysed in a variety of ways. The parts involved in the analysis may be viewed in their undeformed and deformed states, for every analysis step. The analysis may be evaluated in a number of ways. For example contour plots are available and information may be requested in the form of an xy plot.

Pre-processing, solving and post-processing were all executed in ABAQUS® Standard for this investigation.

2.2 Computational Fluid Dynamics

The fundamental basis of computational fluid dynamics are the Navier Stokes equations, which define Newtonian fluid flow. CFD is a computational proce ss, which solves these equations approxmimately using the finite element, finite volume or finite differencing methods. FLUENT® , in particular, uses the finite volume method, which applies the governing equations on discrete volumes, conserving certain properties [10].
CFD is performed in the following three steps:

1. Pre-processing:
   In the pre-processor (GAMBIT® was used for this investigation) the flow domain is defined and divided into a number of volumes or cells (by a process called meshing). Boundary entities, including various inlets and outlets, are specified in this step, so that variables, such as temperature, velocity and pressure can be evaluated at the nodes within the control volumes [10].

2. Solver:
   The governing equations, the Navier Stokes, are integrated over all of the control volumes in the domain, with regard to mass, momentum and, in some cases, energy conservation. The equation is then discretised via the substitution of the approximations into the governing flow conditions. Either an iterative or direct method is then used to solve the resulting algebraic equations [10].

3. Post-processing:
   The results of the solved equations may be viewed in a number of ways, depending on the specific purpose of the programmer. One can view the results as contour or vector plots, xy data plots etc.

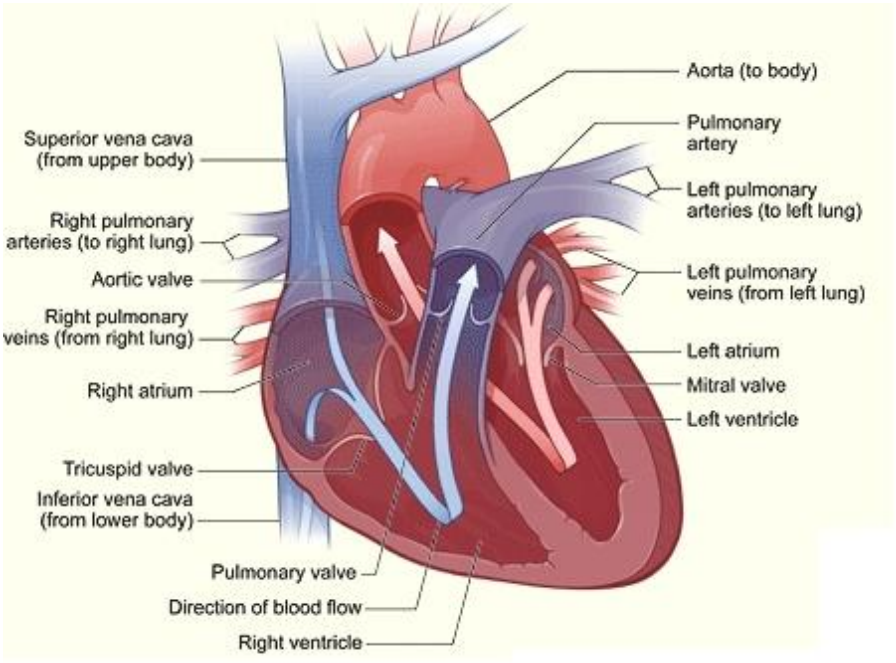

Figure 2.1: Circulation of blood through the heart and to the body (courtesy of [2])

2.3 The circulatory system and the ascending aorta

The heart is comprised of four chambers, the left and right atria and the left and right ventricles. De-oxygenated blood, from the body, enters the right atrium and is transported to the right ventricle via the tricuspid valve. The blood is then pumped through the pulmonary artery, which branches to the left and right lungs, where the blood is oxygenated. From the lungs the blood is transported to the left atrium via the pulmonary veins. From here the mitral valve allows blood to flow from the left atrium to the left ventricle, from where the blood is pumped through the aorta to all of the body's limbs and organs (except the lungs). The de-oxygenated blood then returns to the right atrium by the venous system to complete the cycle, which is then repeated. [2] This system is shown in Figure 2.1.

Blood is pumped into the body by the heart muscle. As the heart muscle contracts, pushing blood out, the blood pressure reaches its peak value (a value around $120mm$Hg is considered normal) and this is called systole. When the heart expands with blood, the lowest value of blood pressure is reached (a value near $80mm$Hg is considered normal) and this is called diastole [11].

The aorta is the largest artery in the human body and consists of three sections; the ascending aorta, the aortic arch and the descending aorta. The ascending aorta is the first section of the aorta and extends obliquely upward, anteriorly and to the right for about five centimetres to the aortic arch. Changes in the mechanical properties in this section of the aorta can have an impact on the entire body [2].

2.4 Numerical investigations of arteries

A number of biomechanical studies have focused on the human artery, with various points of focus. In his investigation, Perktold [12] focused on the effect of distensibility of the artery wall on local blood flow in the carotid artery bifurcation. He noted the relationship between the progress of the disease atherosclerosis as related to an irregular flow field in arteries. This irregular flow field was attributed to curvature in areas of the arterial system.
His model involved an incrementally linear elastic wall and a non-Newtonian incompressible fluid. The flow and wall behaviour were analysed using CFD and the FEM respectively, and an iterative coupling procedure was applied to fully solve the problem. The model was three-dimensional as the bifurcation geometry caused secondary motion, which would not have been captured by a two-dimensional model [13], [14]. The rheology of blood was incorporated into the model with a multi-parameter shear thinning model and the blood flow was pulsatile [15].

Another study coupling blood flow and artery wall mechanics was executed by Geng Gao et al [16]. A three-dimensional layered model of the aortic arch was developed, including the adventitia, media and intima. The walls were approximated as linearly elastic and a FEM anaylsis was carried out, while the flow was pulsatile, and the wall/fluid mechanical interaction was analysed using computational loose coupling fluid structure interaction analyses.

Pedrizzetti et al [17] modelled pulsatile flow in elastic arteries to find the effects of this wall elasticity on flow. The artery was modelled as being a circular conduit, and the blood/wall interaction was evaluated via a perturbative method. The model was axi-symmetric due to the circular nature of the geometry and attention was placed on the lag between pressure and flow in the artery.

An investigation of abdominal aortic aneurysms was performed by Silber et al [8] The focus was on the flow and deformation in an aneurysm. The CFD code /fluent and the FEM code ABAQUS® were used for the investigation and the two codes were coupled using MpCCI. The arterial wall was modelled as hyperelastic [18] and isotropic and the non-Newtonian aspect of blood was modelled using a Carreau model [19]. Blood flow was modelled as steady, as a transient simulation was foreseen to be too time consuming.

A number of independent flow models have been developed [20], [21], [22] [23], which approximate the artery wall as being rigid. Morris et al [24] developed one of these models. The structural model represented the entire aorta and emphasis was placed on the effects of geometry on the three dimensional model. The fact that the model was three-dimensional was imperative due to the complex geometry and the possible three-dimensional flow effects of this geometry.
The data in the study was based on CT/MRI scans while various model simplifications were made. These include the modelling of a constant circular cross section based on the assumption of Shahcheragi et al [25]. Blood flow was modelled both as steady and unsteady to assess how these aspects affected influenced the flow regime. Flow was modelled as laminar and the inlet flow profile was modelled as flat. Blood was approximated as Newtonian, homogeneous and incompressible with constant viscosity and density values. FLUENT® was used as the CFD solver and GAMBIT® as the pre-processor.

Chapter 3

Aortic Wall Models

A number of material models were investigated using a bottom-up engineering approach. The object of this process was to investigate how the various material properties of the ascending aortic wall affect its compliance characteristics. The models start with the simplest case and build, step by step, a more realistic model. The models range from a young and healthy ascending aorta to a diseased aorta affected by arteriosclerosis.

The chapter begins with an introduction to the theory describing the physiological conditions of artery walls. The numerical modelling as performed in this investigation is then described, beginning with a description of the aspects common to all the models used. The individual ABAQUS® models are then detailed, starting with the models of a healthy aorta and concluding with the aged/diseased model.

3.1 Physiology of arterial walls

3.1.1 Geometry of the ascending aorta

The ascending aorta is approximately five centimetres in length with a diameter varying between 20 and 25mm along its length [26]. The aorta is made up of three layers, with a combined (but not constant) thickness of approximately 2mm [27]. These three layers of the aorta are common to all arteries in the body, but vary in size and thickness in the different blood vessels. The innermost layer, the intima (tunica intima), is very thin and almost negligible in a healthy young artery [3], the outermost layer, the adventitia (tunica externa), makes up approximately one third of the total thickness, and the middle layer, the media (tunica media), is the thickest portion of the ascending aortic

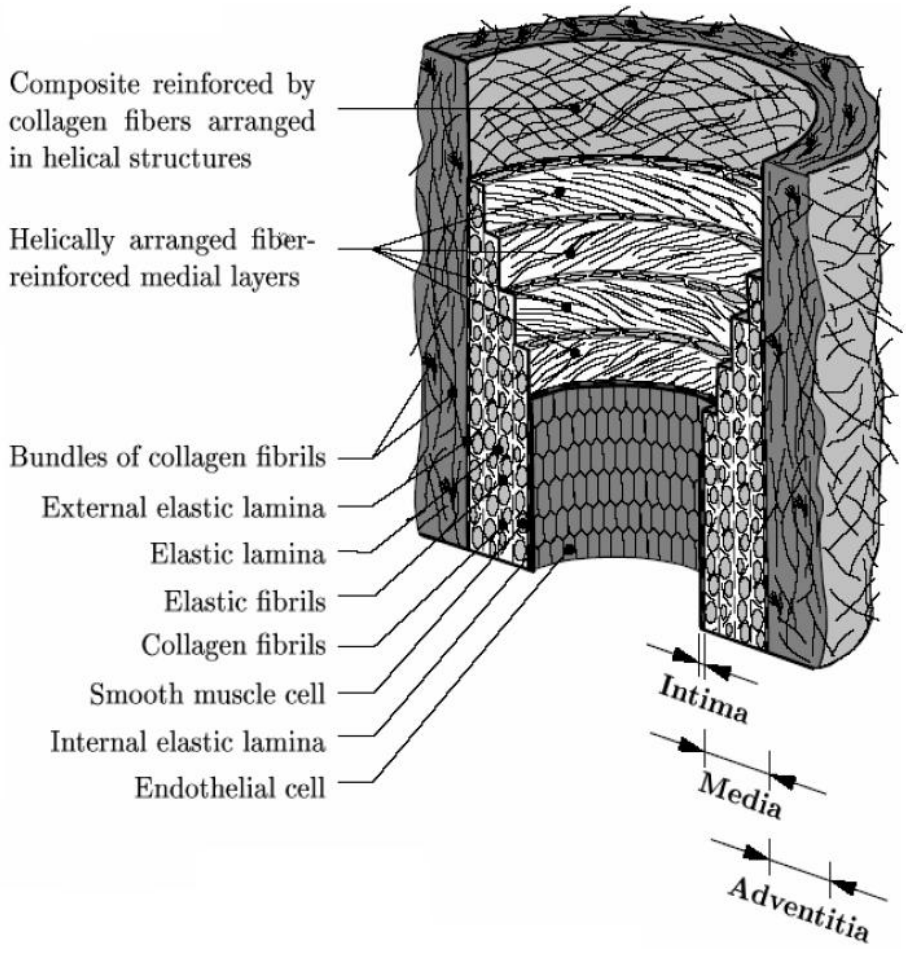

Figure 3.1: Microscopic structure of an elastic artery showing the three layers: tunica intima, tunica media and tunica externa [3]

wall [28]. The three layers are shown in Figure 3.1 below.

3.1.2 Material behaviour of the aortic wall

Each of the three layers of the ascending aorta have different non-linear elastic properties. Artery walls are viscoelastic, which means that they behave simultaneously as both liquid and solid. Ideal fluids will flow when subjected to a shear field, and stop flowing as soon as the stress is removed. An ideal solid subjected to a shear field deforms, and if the stress is removed will recover its original shape immediately (in accordance with Hooke's law), the combination of these properties existing in a viscoelastic material enable the material to exert normal stress [29].

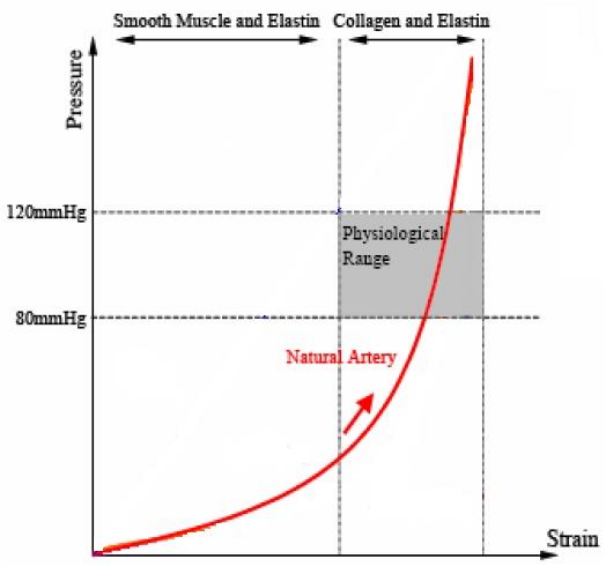

Figure 3.2: Pressure-strain relationship of a healthy artery under loading. (Modified from [4])

The elastic stiffness of arteries increases non-linearly as the load increases. At systole (when the heart contracts) the arteries expand passively with blood, at diastole (when the heart dilates) the arteries recoil elastically, causing the blood to be forced along the arteries. This elastic recoil is the driving force of circulation and reduces the demand on the heart to pump blood round the body. The particular non-linearity of the arterial wall allows stable inflation of the vessel such that a small increase in pressure does not cause a sudden large increase in radius [11]. The non-linear behaviour with loading of a healthy artery is shown in Figure 3.2.

The three concentric layers of the arterial wall as discussed in Section 3.1.1 all exhibit this non-linear behaviour, but with varying levels of stiffness. The innermost layer, the intima, is the stiffest and the adventitia the least stiff of the three. The combined properties of the layers are non-linear, and a certain degree of load transfer between the layers results in the elastic recoil [11].

3.1.3 Mathematical model of the arterial wall

Various constitutive equations describing the material behaviour of soft, biological tissues have been developed. For this investigation, the focus was on a model developed by

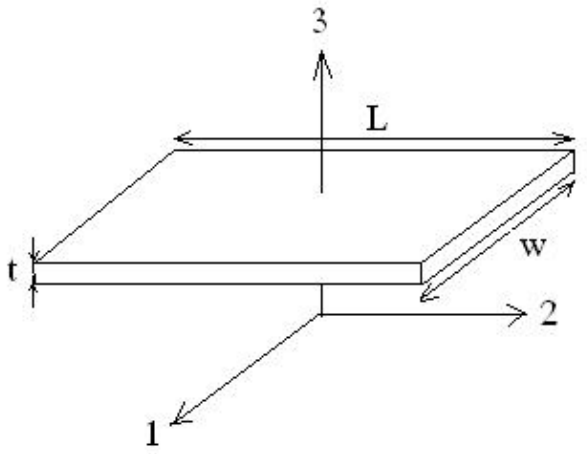

Figure 3.3: Axis system for Holzapfel's material model

Holzapfel [30]. Holzapfel's model was based on the constitutive theory of finite hyperelasticity, combining neo-Hookean and Fung-type strain energy functions. The model was developed from the results of uniaxial extension tests and histostructural data. These tests were performed on the individual layers (intima, media and adventitia) of a healthy human ascending aorta.

The mathematical model was of a transversely isotropic material. In uniaxial tensioning, the tensor in the direction normal to the plane becomes zero for an axis system as in Figure 3.3.

The strain energy, Ψ, completely defines the material and is expressed as a function of the Green-Lagrange strain tensor, $\mathbf{E}$, and is made up of both an isotropic component and a orthotropic component:

$$\Psi = \Psi_{iso}(\varepsilon) + \Psi_{ortho}(\varepsilon). \tag{3.1}$$

The isotropic component of the strain energy governs the initial stiffness of the artery, while the orthotropic contribution governs the much higher stiffness at high strains. Plane stress was assumed and therefore these components are functions of only E_{11} and E_{22}, yielding:

$$\Psi = \Psi_{iso}(\varepsilon_{11}, \varepsilon_{22}) + \Psi_{ortho}(\varepsilon_{11}, \varepsilon_{22}) \tag{3.2}$$

The Holzapfel model went on to assume incompressibility ($\nu = 0.5$, where ν is Poisson's ratio). The isotropic component of strain energy is shown to be given by:

$$\hat{\Psi}_{ortho} = \frac{\mu}{2} 2(\varepsilon_{11} + \varepsilon_{22}) + [(2\varepsilon_{11} + 1)(2\varepsilon_{22} + 1)]^{-1} - 1 \tag{3.3}$$

The orthotropic contribution of the strain energy adopts a exponential "Fung-type" strain energy function [31]. This incorporates four constitutive parameters C, c_{11}, c_{12} and c_{22} where C is a stress-like parameter, while c_{11}, c_{12} and c_{22} are dimensionless [31] Thus,

$$\hat{\Psi}_{iso} = C[e^{Q} - 1] \tag{3.4}$$

where:

$$Q = c_{11}\varepsilon_{11}^2 + c_{12}\varepsilon_{11}\varepsilon_{22} + c_{22}\varepsilon_{22}^2 \tag{3.5}$$

The stress then becomes:

$$\sigma_{11} = \frac{\partial\hat{\Psi}(\varepsilon_{11}, \varepsilon_{22})}{\partial\varepsilon_{11}} \tag{3.6}$$

$$\sigma_{22} = \frac{\partial\hat{\Psi}(\varepsilon_{11}, \varepsilon_{22})}{\partial\varepsilon_{22}} \tag{3.7}$$

and

$$\sigma_{33} = 0 \tag{3.8}$$

The four constants (C, c_{11}, c_{12} and c_{22}) were obtained by a rigorous curve fitting process, to yield the values shown in Table 3.1.

Layer	μ (kPa)	C (kPa)	c_{11}	c_{12}	c_{22}
Intima	39.8	1.42	999.0	510.0	127.0
Media	31.4	0.14	32.8	14.7	23.5
Adventitia	17.3	4.71E-04	37.7	58	63.8

Table 3.1: Material constants describing artery walls as derived by Holzapfel [30]

3.1.4 Effect of arteriosclerosis on the aorta

Age affects the arteries in a number of ways, and a condition known as arteriosclerosis is often a result of the aging process. The main effect is a reduction in compliance of the arteries due to a thickening of the intimal layer. As the intima has the stiffest characteristics of the three layers (as can be seen in Table 3.1), thickening can drastically reduce the arterial compliance. The result of this is that the elastic recoil as discussed in Section 3.1.2 is less effective and there is a more substantial strain on the heart muscle. Arteries may also become brittle with the aging process, increasing the chances of rupture, which can occur during corrective surgery, sometimes having fatal results [32].

3.1.5 Compliance

Compliance is the percentage change in diameter of the artery for a pressure equivalent to $100mm$Hg, thus it is a measure of elasticity of the artery. The mathematical formula for compliance is:[33]

$$C_d = \frac{\Delta D}{D_d \Delta P} 10^4. \tag{3.9}$$

Compliance values in the ascending aorta range between $16.7\%/100mm$Hg with an uncertainty of $\pm 84\%$ [34] to $37\%/100mm$Hg with an uncertainty of $\pm 25\%$ [35]. This large range is due to different testing methods, but it is generally accepted to expect a compliance value between 20% and 25% [32].

3.2 Numerical models as used in this investigation

For each model the geometry, material parameters and boundary conditions and surface interactions of the models will be described in the following sections. Any aspects specific to the individual models will be further explained in the corresponding section.

3.2.1 Common geometrical aspects

The ascending aorta was simplified to resemble a straight cylinder, and therefore the entire problem was assumed to be axi-symmetric. The cylinder had a length (parallel to the flow direction) of $50mm$ and an internal diameter of $12.05mm$. This diameter corresponded with the geometrical condition at diastole. This simple geometrical offset acted as the pre-tension in the aorta, which was sufficient as the material was modelled as linearly elastic throughout and therefore independant of the deformation history. The initial thicknesses of the media and adventitia were set at $1.2mm$ and $0.6mm$ respectively, thus the combined thickness of the two layers was $1.8mm$ in agreement with Gao's model [16]. The geometry is shown in Figure 3.4

3.2.2 Boundary conditions and surface interactions

Boundary conditions fix certain motion or applied tractions, while interactions specify contact relationships between two components or materials. In the models, the only type of interaction used was the elastic foundation, which was used to model the effects of surrounding fatty and muscular tissue. This acts as a series of springs, in parallel, along the length of the relevant surface with a stiffness per unit area, (k/A) specified

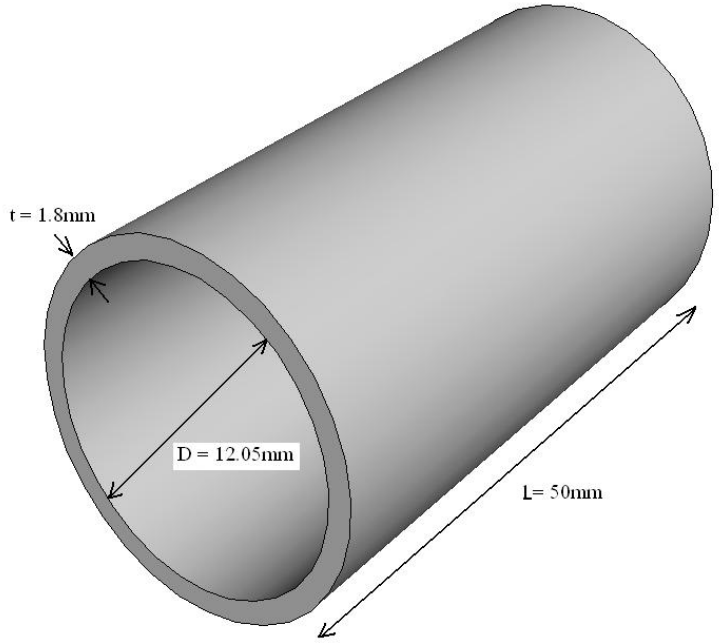

Figure 3.4: Geometry of modelled ascending aorta

by the user. These springs approximate another material or deformable part in direct contact with the modelled solid. The stiffnesses were evaluated as follows:
For linear elasticity

$$E = \frac{\sigma}{\varepsilon}$$

where $\sigma = \frac{F}{A}$ and $\varepsilon = \frac{\Delta L}{L_{init}}$, thus:

$$E = \frac{FL_{init}}{A\Delta L}$$

but, according to Hooke's law

$$k = \frac{F}{\Delta L}$$

therefore

$$E = \frac{kL_{init}}{A}$$

and thus the stiffness per unit area:

$$k/A = \frac{E}{L_{init}} \tag{3.10}$$

The boundary conditions and surface interactions for the models are as follows:

1. **At inlet:**
   No displacement was allowed in the axial direction ($u_z = 0$)
   No rotation was allowed in the circumferential direction ($\theta_z = 0$)

2. **At outlet:**
   An elastic foundation was specified, such that the ascending aorta may "shorten" but not freely, with the stiffness per area such that it was equivalent to there being $50mm$ of aortic material extending from it.

3. **Along the length of the aorta:**
   Two different elastic foundations were specified along the length of the aorta, for $1mm$, $k/A = 8000Pa/m^2$ and for the rest of the length $k/A = 4000Pa/m^2$.

The inlet condition constrains the aortic model where it was "connected" to the left ventricle, and assumed that the area in direct contact would not move away from the ventricle (condition 1).
The interaction acting on the first $1mm$ after inlet to the aorta (as mentioned in condition 3) acted as a cylinder encompassing the beginning of the aorta, allowing it to expand in a constrained fashion.

The outlet of the ascending aorta model was allowed to move in any direction (condition 2), but was restrained from an uncontrolled axial shortening by an interaction mimicking an extension of aortic material for $50mm$, which was the modelled aorta length again. This interaction was specified to mimic, to some extent, the support of the aortic arch, descending aorta and the rest of the system.

As the aorta is supported by various biological tissues and fluids within the myocardium, the model needed to be constrained along its length in some way (condition 3). The combination of these media were approximated as a $2.5mm$ thick layer of fat, following the example set out by Janoske et al [8].

The layers of the aorta were modelled as one entity, with the total thickness partitioned into layers with material properties specific to the relevant sections of the aorta (intima, media and adventitia), rather than separate parts modelled in full contact with one another. This modelling technique was used to ensure that any deformation of the vessel did not cause any separation between the layers as a result of the soft and hard contact methods of employed by ABAQUS® . For the hard contact specification, the penetration of one surface into the other is minimised, and as soon as the contact pressure reduces to zero, the surfaces will separate. This presents the risk of a loss of contact. When soft contact is specified, a force exists between the surfaces as a function of the distance between the surfaces. Because this force exists, actual contact between

the surfaces may never actually occur. Using an elastic foundation also obviates the existence of two deformable parts, and consequently two meshes, thus simplifying the solution of the matrix. The boundary conditions are shown in Figure 3.5.

3.2.3 Loading conditions on the aorta

As previously discussed, the aorta was modelled during diastole, therefore for the independantly run solid simulations only the difference in pressure from diastole to systole (equivalent to $40mm$Hg) was applied to the aorta. This load was applied as a uniform pressure along the entire inner wall of the artery creating the condition as shown in Figure 3.5.
For the coupled simulations the loading is as described in Chapter 5.

3.2.4 Development of constitutive equations

As previously discussed blood vessels are viscoelastic (see Section 3.1.2), in this investigation, the ascending aorta was analysed within the linear range of elasticity. The material model was obtained by the linearisation of the constitutive equations as discussed in Section 3.1.3 which takes the transverse isotropic nature of arteries into account.

The model discussed in Section 3.1.3, described the strain energy, Ψ, as consisting of the sum of two components, one isotropic, $\Psi_{iso}(\varepsilon)$, and one orthotropic, $\Psi_{ortho}(\varepsilon)$. The material was approximated as being incompressible ($\nu = 0.5$), and the model defined a hyperelastic material, however, for a linear elastic model, material stability requires that the tensor D^{el} be positive definite and thus there exist certain restrictions on the material constants.
The assumption of incompressibility led to this instability and therefore the material was instead modelled as being near-incompressible, with $\nu = 0.45$.
The isotropic component from the Holzapfel model was discarded and was instead developed incorporating the Lamé moduli, where:

$$\lambda = \frac{\mathrm{E}\nu}{(1+\nu)(1-2\nu)} \tag{3.11}$$

and

$$\mu = \frac{\mathrm{E}}{2(1+\nu)} \tag{3.12}$$

It can be seen from Equation 3.11 how the assumption of incompressibility lead to a zero denominator in λ and why the near-incompressible model was necessary.

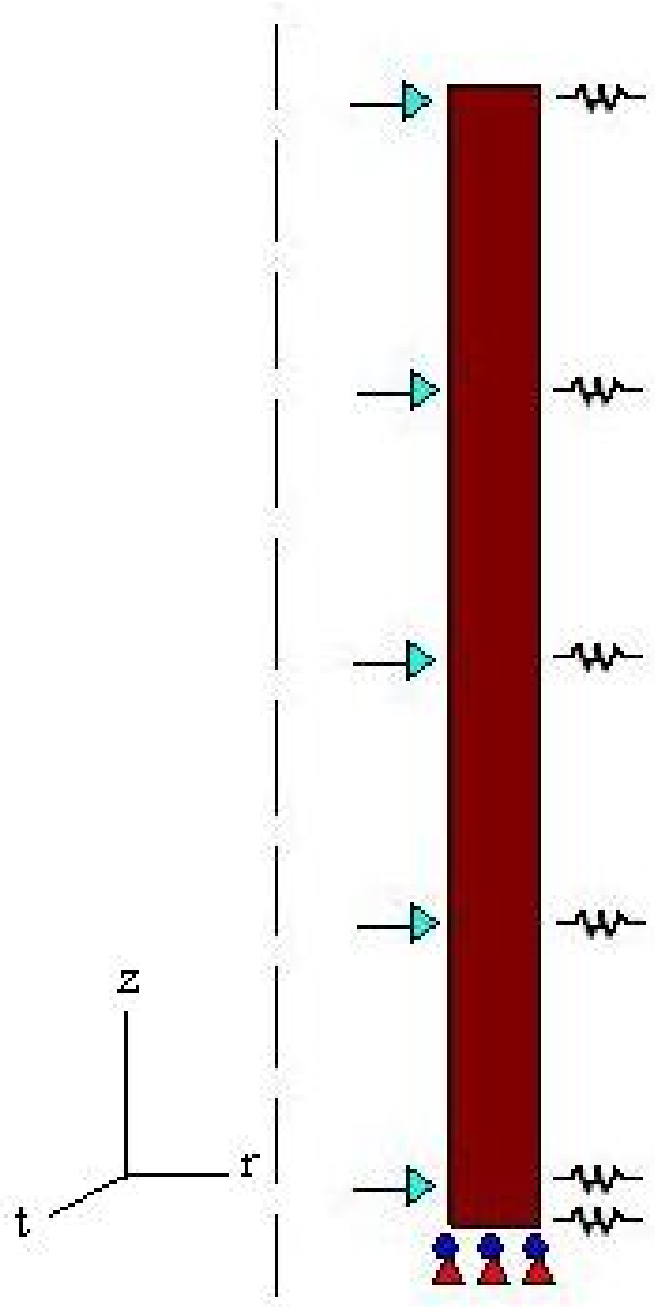

Figure 3.5: Boundary conditions, surface interactions and loading conditions on the models

Thus the isotropic stress component of the material, as a function of strain, was:

$$\sigma = \lambda(E_{11} + E_{22} + E_{33})(\mathbf{I}) + 2\mu((\mathbf{E}) \tag{3.13}$$

where (**I**) is the identity matrix.

The orthotropic component of Holzapfel's model was linearised via a Taylor expansion to the first degree, and added to the above isotropic component. The linearisation led to the following stress definitions:

$$\sigma_{11} = \sigma_{11}(0) + \alpha_{11}\varepsilon_{11} + \alpha_{22}\varepsilon_{22} \tag{3.14}$$

$$\sigma_{22} = \sigma_{11}(0) + \beta_{11}\varepsilon_{11} + \beta_{22}\varepsilon_{22} \tag{3.15}$$

where

$$\alpha_{11} = \left.\frac{\partial\sigma_{11}}{\partial\varepsilon_{11}}\right|_0 \tag{3.16}$$

$$\alpha_{22} = \left.\frac{\partial\sigma_{11}}{\partial\varepsilon_{22}}\right|_0 \tag{3.17}$$

$$\beta_{11} = \left.\frac{\partial\sigma_{22}}{\partial\varepsilon_{11}}\right|_0 \tag{3.18}$$

$$\beta_{22} = \left.\frac{\partial\sigma_{22}}{\partial\varepsilon_{11}}\right|_0 \tag{3.19}$$

and

$$\sigma_{11} = \frac{\partial\Psi}{\partial\varepsilon_{11}} \tag{3.20}$$

$$\sigma_{22} = \left.\frac{\partial\Psi}{\partial\varepsilon_{22}}\right|_0 \tag{3.21}$$

This gives:

$$\alpha_{11} = 4\mu + 2c_{11}C \tag{3.22}$$

$$\alpha_{22} = 2\mu + Cc_{12} = \beta_{11} \tag{3.23}$$

$$\beta_{22} = 4\mu + 2c_{22}C \tag{3.24}$$

The components were transformed into an equivalent cylindrical coordinate system such that the subscripts 1, 2 and 3 are equivalent to r, z and θ respectively and summed

to give

$$\begin{bmatrix} \sigma_{rr} \\ \sigma_{zz} \\ \sigma_{\theta\theta} \\ \tau_{rz} \\ \tau_{r\theta} \\ \tau_{z\theta} \end{bmatrix} = [D] \begin{bmatrix} \varepsilon_{rr} \\ \varepsilon_{zz} \\ \varepsilon_{\theta\theta} \\ \gamma_{rz} \\ \gamma_{r\theta} \\ \gamma_{z\theta} \end{bmatrix} \tag{3.25}$$

where:

$$[D] = \begin{bmatrix} \alpha_{11}+\lambda+2\mu & \alpha_{22}+\lambda & \lambda & 0 & 0 & 0 \\ \beta_{11}+\lambda & \beta_{22}+\lambda+2\mu & \lambda & 0 & 0 & 0 \\ \lambda & \lambda & \lambda+2\mu & 0 & 0 & 0 \\ 0 & 0 & 0 & 2\mu & 0 & 0 \\ 0 & 0 & 0 & 0 & 2\mu & 0 \\ 0 & 0 & 0 & 0 & 0 & 2\mu \end{bmatrix} MPa \tag{3.26}$$

The constants were dealt with in a way specific to each model, which will be discussed in the sections on the individual models.

3.2.5 Meshing of the models

The models were all meshed in the same manner as they all needed to be compatible with the fluid model mesh. It was necessary that the mesh be fine enough to capture any relevant information in the running of the job. On the other hand an excessively fine mesh was avoided so as to keep the compatibility of the fluid and solid grids as simple as possible. It was found that 200 elements along the common boundary was sufficient for this problem, with an equivalent spacing along the two boundaries perpendicular to the axis of symmetry. This resulted in 0.25mm spacing between the nodes. A free meshing technique was adopted, as it was found that this allowed the greatest control according to the edge seeding. The meshed part is shown in the section specific to the individual model. The elements used were axisymmetric stress elements, which is the default element type for axisymmetric models in ABAQUS® . This element type allows only isotropic or orthotropic material properties, and loading only in the radial and axial directions. If a radial displacement occurs, this will cause a “hoop” strain, which is a strain in the circumferential direction.

3.2.6 Models of a healthy, young ascending aorta

In a healthy artery the intima is "very thin" [3] and thus the effect of this layer on the solid mechanical properties is assumed to be insignificant. Consequently the models analysed in this subsection neglected this layer entirely, with only the material and geometrical properties of the media and adventitia being included.

Single layer, isotropic model

Geometry: The geometry of the aorta is that shown in Figure 3.4, with the combined thickness of the two relevant layers used as the entire wall thickness (1.8 mm). The ascending aorta model is five centimetres long with an internal diameter of 12.5 mm as used in [16].

Material: The first model created was linear elastic, isotropic and consisted of only a single layer. The elastic modulus of this layer was derived as a weighted average of the elastic moduli found for the two layers, according to the area of each of the layers in the cross section of the ascending aorta as follows:

$$E_{ave} = \frac{2}{3}E_{media} + \frac{1}{3}E_{adventitia} \tag{3.27}$$

as the media makes up two thirds and the adventitia makes up one third of the total cross sectional area of the ascending aorta (see Figure 3.6 in Section 3.2.6), and E was found from Equation 3.12.

As the material is isotropic, the constants in the orthotropic component of the mathematical model were set to zero:

$$c_{11} = c_{12} = c_{22} = 0 \tag{3.28}$$

while all the others were maintained as those in Table 3.1. The elastic modulus of the isotropic material was $0.07794 MPa$ and had a D-matrix of:

$$[D] = \begin{bmatrix} 0.2937 & 0.2403 & 0.2403 & 0 & 0 & 0 \\ 0.2403 & 0.2937 & 0.2403 & 0 & 0 & 0 \\ 0.2403 & 0.2403 & 0.2937 & 0 & 0 & 0 \\ 0 & 0 & 0 & 0.0534 & 0 & 0 \\ 0 & 0 & 0 & 0 & 0.0534 & 0 \\ 0 & 0 & 0 & 0 & 0 & 0.0534 \end{bmatrix} MPa \tag{3.29}$$

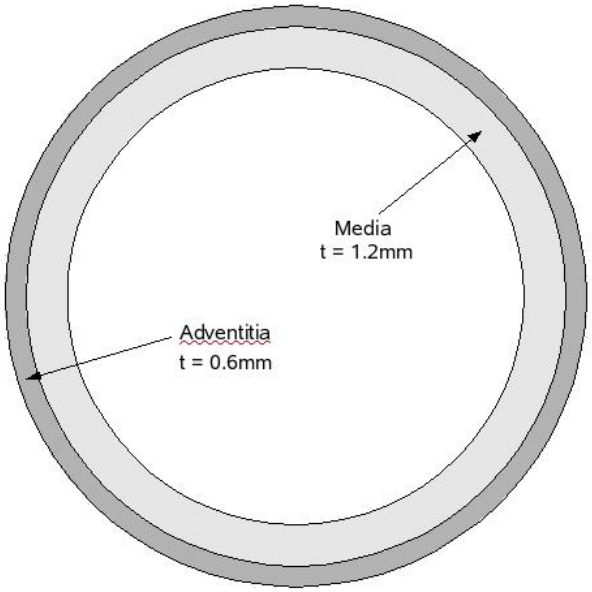

Figure 3.6: Cross section of healthy artery showing the thicknesses of the medial and adventitial layers

Boundary conditions and surface interactions: The boundary conditions described in Section 3.2.2 hold for this model. The elastic foundation at the aortic outlet has a stiffness per area of $1548.6 Pa/m^2$, which represents a continuation of the material properties as for the rest of this model. The interaction property values in all other regions of the model are as set out in Section 3.2.2.

Double layer, isotropic model

Geometry: This model consisted of two layers; the media, being 1.2mm thick, and the adventitia, being 0.6mm thick. All geometrical aspects of this model are as discussed in Section 3.2.1 and the cross section is shown in Figure 3.6.

Material: As in the single layer, isotropic model (Section 3.2.6), the material model was isotropic. Therefore the constants in the orthotropic component of the material model were zeroed:

$$c_{11} = c_{12} = c_{22} = 0 \tag{3.30}$$

for all of the layers. The various material constants are shown in Table 3.1, and were assigned to the relevant layers, yeilding a D-matrix as follows:

$$[D] = \begin{bmatrix} 0.3454 & 0.2826 & 0.2826 & 0 & 0 & 0 \\ 0.2826 & 0.3454 & 0.2826 & 0 & 0 & 0 \\ 0.2826 & 0.2826 & 0.3454 & 0 & 0 & 0 \\ 0 & 0 & 0 & 0.0628 & 0 & 0 \\ 0 & 0 & 0 & 0 & 0.0628 & 0 \\ 0 & 0 & 0 & 0 & 0 & 0.0628 \end{bmatrix} MPa \tag{3.31}$$

for the medial layer, with $E = 0.09106Mpa$, and

$$[D] = \begin{bmatrix} 0.1903 & 0.1557 & 0.1557 & 0 & 0 & 0 \\ 0.1557 & 0.1903 & 0.1557 & 0 & 0 & 0 \\ 0.1557 & 0.1557 & 0.1903 & 0 & 0 & 0 \\ 0 & 0 & 0 & 0.0346 & 0 & 0 \\ 0 & 0 & 0 & 0 & 0.0346 & 0 \\ 0 & 0 & 0 & 0 & 0 & 0.0346 \end{bmatrix} MPa \tag{3.32}$$

for the adventitial layer, with $E = 0.0517$.

Boundary conditions and surface interactions: Once again the elastic models as described in Section 3.2.2 held. The elastic foundation at the outlet was specific to each layer of the aorta, with an extension of the media tissue connecting to the medial layer at outlet and an extension of the adventitia tissue connecting to the adventitial layer at outlet. This resulted in $k/A = 1821.2Pa$ at the media and $k/A = 1034Pa$ at the adventitia. All other interaction properties from Section 3.2.2 held..

Double layer, orthotropic model

Geometry: As in section 3.2.6 the model consisted of two layers, as shown in Figure 3.6. The media is once again 1.2mm thick and the adventitia 0.6mm thick.

Material: The material in this model is orthotropic, with the values of the constants mentioned in section 3.1.2 having the values shown in Table 3.1.

These values result in a D-matrix of:

$$[D] = \begin{bmatrix} 0.345400 & 0.282600 & 0.282600 & 0 & 0 & 0 \\ 0.282600 & 0.354584 & 0.284658 & 0 & 0 & 0 \\ 0.282600 & 0.284658 & 0.351980 & 0 & 0 & 0 \\ 0 & 0 & 0 & 0.062800 & 0 & 0 \\ 0 & 0 & 0 & 0 & 0.062800 & 0 \\ 0 & 0 & 0 & 0 & 0 & 0.062800 \end{bmatrix} MPa \quad (3.33)$$

for the medial layer, with $E = 0.03106 Mpa$ and

$$[D] = \begin{bmatrix} 0.190300 & 0.155700 & 0.155700 & 0 & 0 & 0 \\ 0.155700 & 0.190360 & 0.155727 & 0 & 0 & 0 \\ 0.155700 & 0.155727 & 0.190335 & 0 & 0 & 0 \\ 0 & 0 & 0 & 0.034600 & 0 & 0 \\ 0 & 0 & 0 & 0 & 0.034600 & 0 \\ 0 & 0 & 0 & 0 & 0 & 0.034600 \end{bmatrix} MPa \quad (3.34)$$

for the adventitial layer, with $E = 0.0517 MPa$.

Boundary conditions and surface interactions: Again the boundary conditions and interactions as laid out in Section 3.2.2 hold. The interaction property values are the same as those discussed in Section 3.2.6 above.

3.2.7 Models of an aged/diseased artery

Effects of age and disease

As dicussed in section 3.1.4, arteriosclerosis is caused by a thickening of the intimal layer in the arteries. As the elastic properties of the intima lead to a much stiffer material, this thickening reduces compliance in the arteries. This effect was investigated by adding an intimal layer to the wall model as described in the sections below.
It should be noted that the effects of atherosclerosis would be similar to those of arteriosclerosis, at some level, as the former is a build up of various compounds (cholesterol, calcium, etc), which also cause a stiffening of the artery walls. However, this condition also "clogs" the artery, decreasing the cross sectional area through which the blood must flow, thus further increasing the strain on the heart.

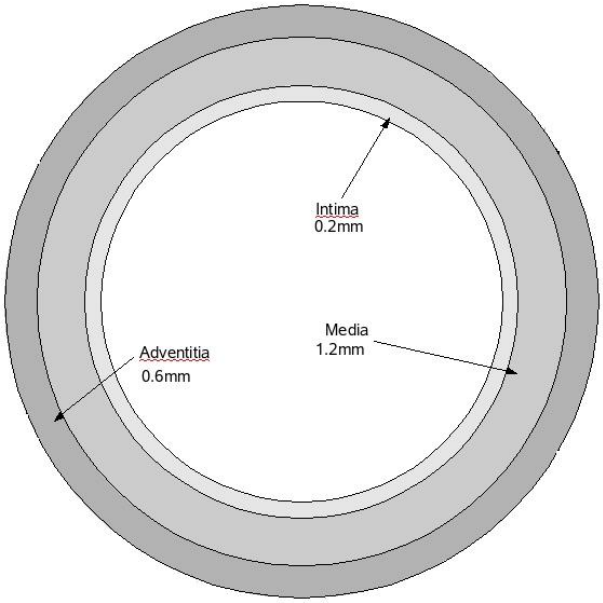

Figure 3.7: Cross section of model affected by arteriosclerosis, with an initial intimal thickening of 0.2mm

Geometry: The model of the artery affected by arteriosclerosis included all three layers; intima, media and adventitia. The inner diameter of the aorta was held at $12.05mm$ to maintain compatibility with the fluid mesh, while the outer diameter became larger as a result of the increasing thickness of the artery wall. The initial model had an intima with a thickness of 0.2mm (as used by Gao et al [16] in a three layer healthy aorta model). The thickness was increased to $0.4mm$ and finally to $0.6mm$, at which point it has the same thickness as the adventitia, to investigate the possible existence of a trend with intimal thickening. Figure 3.7 shows the first model, with the initial intimal thickening condition.

Material: The material model for the medial and adventitial layers was the same as that in Section 3.2.6. The added intimal layer used the constants as shown in Table 3.1 and $E = 0.11542MPa$. The D-matrix for the two outer layers were as in Section 3.2.6,

while that of the intimal layer was:

$$[D] = \begin{bmatrix} 0.437800 & 0.358200 & 0.358200 & 0 & 0 & 0 \\ 0.358200 & 0.288094 & 0.760020 & 0 & 0 & 0 \\ 0.358200 & 0.760020 & 0.404460 & 0 & 0 & 0 \\ 0 & 0 & 0 & 0.079600 & 0 & 0 \\ 0 & 0 & 0 & 0 & 0.079600 & 0 \\ 0 & 0 & 0 & 0 & 0 & 0.079600 \end{bmatrix} MPa \quad (3.35)$$

.

Boundary conditions and surface interactions: The boundary conditions and surface interactions as described in Section 3.2.2 held, with the elastic foundation at the outlet being that of each layer extending for $50mm$. The surface interaction properties for the media and adventitia at outlet were the same as those in Sections 3.2.6 and 3.2.6. The intima outlet interaction had a value of $k/A = 2308.4Pa$.

Chapter 4

Blood Flow Models

A single blood flow model was developed and used for every wall model. The details of the modelling process will be laid out in this chapter, introduced by a review of literature on the subject. The modelling process is then described in the following sections.

4.1 Blood flow in the ascending aorta

Blood is a very complex fluid, and the pulsatile nature of blood flow in the human body adds still more complexity to the modelling of this flow, however there are various assumptions which may be made to greatly simplify this problem.

4.1.1 The material properties of blood

Blood is a non-Newtonian fluid, a class of fluids including all fluids that have behaviour deviating from Newton's laws. In a Newtonian fluid, the rate of deformation of the fluid and the stress applied to it are directly proportional, that is, the fluid obeys Newton's law of constant viscosity. A non-Newtonian fluid, like blood, has a non-linear response to stress; the stress in the fluid is dependant on both the instantaneous deformation and the instantaneous rate of change of the deformation [29]. This greatly affects the behaviour of blood in arteries, however it is reasonable to model blood as a Newtonian fluid when dealing with large, elastic arteries [24] and, as the aorta is the largest artery in the human body, this assumption applied to this investigation.

4.1.2 Blood flow characteristics

Flow in arteries is pulsatile, which may cause the flow to become turbulent, thus an investigation into this possibility was conducted by Morris et al [24]. Accelerating flow is more stable and decelerating flow less stable than steady flow, therefore there is a possibility of bursts of turbulence in the decelerating phase of the pressure pulse [36], [37]. In another investigation, conducted by Nerem et al [38], a critical Reynolds number for unsteady flow was found. For the model used by Morris et al [24] the maximum Reynolds number (for the decelerating flow phase) was below this critical value and thus the flow was assumed to be laminar.

4.1.3 Laminar flow

When a fluid flows along a surface the friction between the surface and the fluid causes there to be no relative motion between the surface and the fluid that is in direct contact with it. As a result of this, a velocity gradient exists between the fluid at the surface and the fluid far away from the surface (i.e. that in the free stream). In fully developed pipe flow the flow profile approximates a parabola, due to the increasing velocity with distance from the wall, and the shape of this parabola is determined by the viscosity of the fluid.

4.2 Grid geometry and boundary conditions

As the ascending aorta was approximated as cylindrical, with a constant cross section, the flow was assumed to be axi-symmetric. FLUENT® calculates the results of axi-symmetric problems by integrating over 2Π radians. The geometry for the flow domain of the aorta was defined in GAMBIT® . A rectangular domain was created and meshed, as shown in Figure 4.1.

Four boundary types were assigned as follows:

- The common boundary between the solid and fluid meshes was defined as a “wall” boundary, which contains the fluid and defaults to a no slip condition.
- The centre line of the aorta was defined as an “axis” boundary, which assigns it axis of symmetry properties, and does not require the specification of any other boundary conditions.

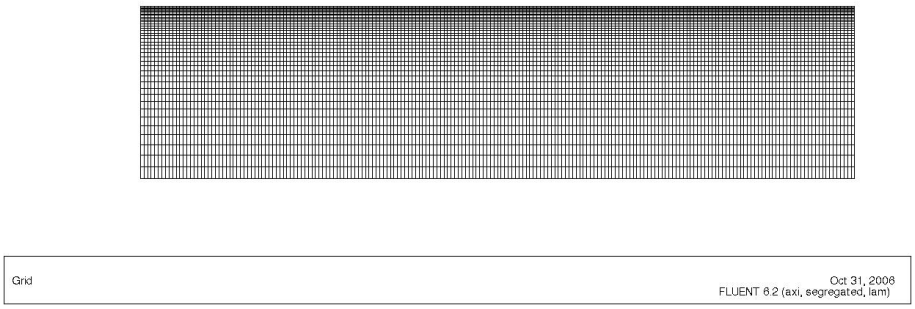

Figure 4.1: Meshed grid used for CFD analysis

- The inlet boundary was assigned a "velocity inlet" boundary type as the information available described an inlet value [24]. This type of boundary is suitable for incompressible flow. The inlet velocity profile will be described in section 4.6.
- At the outlet, no information was known, and therefore an "outflow" boundary type was assigned, which is also appropriate for incompressible flow. For this type of boundary, FLUENT® extrapolates the required information from the interior.
- The fluid within the boundaries assumed the default "interior" boundary type.

The mesh consisted of bilinear quadrilateral elements, created by the "map" meshing scheme, which creates a structured, regular grid. The grid was refined in the area close to the artery wall so as to monitor boundary layer phenomena. The refinement was graded according to an exponential function with a ratio value of 0.32. A total of 40 elements were created along the inlet and outlet boundaries of the aorta. The elements along the wall and axis boundaries were evenly spaced for 200 elements.
As discussed in Section 3.2.5 it was essential to have a grid fine enough to capture any relevant flow phenomena but also it was necessary to maintain compatibility with the solid mesh. The nodes on the fluid domain wall boundary fell on the same points as the nodes on the solid boundary.

4.3 General properties of model

As discussed in Section 4.1, blood flowing through the aorta can be approximated as Newtonian, therefore, the density and viscosity were set as constant, with values of

$1050kg/m^3$ and $0.0035Pas$ respectively and the fluid was assumed incompressible [16], [24].

4.4 Operating Conditions

Due to the fact that the wall model had an initial condition of diastolic pressure, the initial pressure induced in the artery had to be representative of the flow conditions at systole. Therefore the operating conditions were set at the systolic condition, with an operating (guage) pressure of $120mm$Hg. The reference point was set at the inlet to the aorta at the vessel wall (i.e. on the common boundary).

4.5 Flow characteristics as defined in Fluent

The flow was defined as axi-symmetric, and therefore an axi-symmetric solver was utilised. A time averaged input velocity as deduced by Morris et al [24] was applied. This inlet velocity was deduced from flow rates obtained from Nichols and Rourke [39]. As discussed in 4.1, the model used by Morris et al [24] was laminar for the decelerating phase of the flow, therefore as steady flow is more stable than flow in the decelerating phase [36], the flow was assumed to be laminar throughout the ascending aorta.

The working fluid was set as blood with the properties discussed in Section 4.3. The default no slip condition at the aorta wall was retained. At the outflow boundary the flow rate weighting was left at the default value of 1, as all the flow exits through the same outlet.

4.5.1 Solution Controls

SIMPLEC (Semi-Implicit Method for Pressure-Linked Equations (Consistent)) was used as the method of pressure velocity coupling and the under-relaxation factors were left at the default values. This solver is an improved version of the SIMPLE algorithm and is ideal for steady state problems [40]. The discretisation scheme utilised was QUICK (Quasi-upwind interpolation for convective kinetics), which interpolates between three data points with an upstream weighting [24]. The increased accuracy due to the extra data point was not foreseen to create any significantly increase the simulation time due to the computational simplicity of the model.

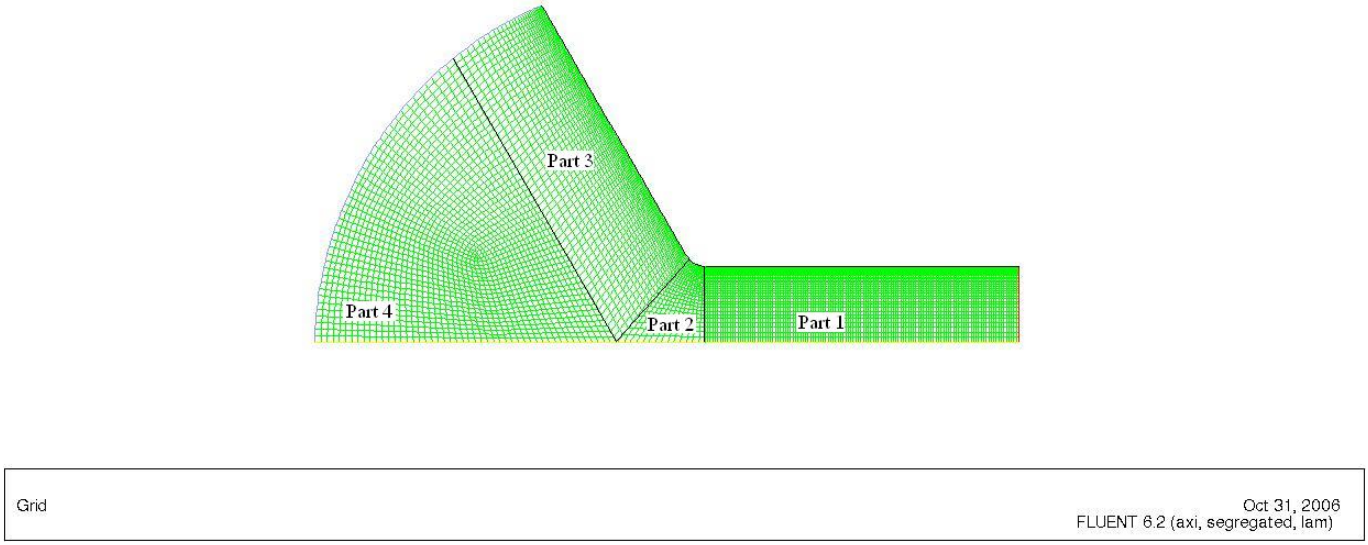

Figure 4.2: Partitions and mesh of investigated inlet velocity profile

4.6 Investigation into the inlet velocity profile

Blood flow into the ascending aorta is controlled by a one-way valve (the aortic valve). The change in flow area from the left ventricle of the heart to the ascending aorta was foreseen to yield a velocity profile at the aorta inlet which was neither completely flat nor parabolic (the case in fully developed laminar flow (see Section 4.1)).
This combination of velocity gradients was expected as a result of the sudden change in flow area, but the extent of the gradients was not known quantitively. However, it was expected, from reports of CT scans [36], [41],[42], [43], [44] that the profile would show a relatively flat velocity profile at the inlet to the aorta.

4.6.1 Geometry and mesh

The geometry of the aorta with the included ventricle is shown in Figure 4.2. The geometric properties of the aorta are the same as those described in Section 4.2. The extension of the left ventricle is by no means an accurate representation, but merely served the purpose of simulating a sudden change in flow area. The radius of the ventricular section was set to five times that of the aorta radius, at $60.25mm$. The section connecting the ventricle to the aorta was angled at 30°, and entry was smoothed with a fillet radius of $3.95mm$ (see Figure 4.2).

The rectangular aortic section was meshed as described in Section 4.2. The ventricle was partitioned as shown in Figure 4.2, to allow the most even mesh possible. Parts 2 and 3 (Figure 4.2)) essentially extend the mesh from Part 1, with an exponentially graded mesh, in keeping with that of Part 1. Due to the quadrilateral shape of these parts, they were meshed with the "map" meshing scheme of GAMBIT® with quadrilateral elements.
It was not imperative that the elements along the inlet boundary of Part 4 were graded as they are sufficiently far away from any surface. 41 evenly spaced elements were set along this edge, and 52 along the axis boundary (which were extended through Part 3). As this section was three sided, GAMBIT® 's "tri-primitive" meshing scheme was utilised. This scheme divides a three sided shape into three quadrilateral regions and uses a "map" scheme to mesh these three regions [40]. A total of 15008 elements were created for this model.

4.6.2 Boundary conditions

The boundary conditions as described in Section 4.2 were applied to the model, except for those at the inlet to the aorta. The inlet to the "ventricle" was assigned the velocity inlet boundary type and the inlet to the aorta/outlet to ventricle was defined as an interior boundary type, to enable the extraction of data at this boundary. The ventricle wall was assigned the wall boundary type and the no slip condition was retained.

Inlet condition

The profile was investigated with a crude geometric model of the left vetricle leading into the diameter of the aorta as shown in Figure 4.2. The average axial velocity at inlet to the aorta was approximated as $0.0035m/s$ [24]. This condition was ensured by the assumption of a constant volume flow rate to the ventricle inlet as shown in Figure 4.2. Continuity in an incompressible fluid is satisfied by:

$$v_{in}A_{in} = v_{out}A_{out} \tag{4.1}$$

where A is the cross-sectional flow area and v is the velocity normal to A, while subscripts "in" and "out" are the values at inlet and outlet respectively, this resulted in a constant velocity value of $0.00354m/s$ at the "inlet" to the ventricle.

4.6.3 Use of profile in final model

The model was run with the flow characteristics as defined in Section 4.5 and the velocity profile was extracted at the aortic inlet. This profile was then programmed into a User Defined Function (U.D.F) which was included in the boundary condition at the aorta inlet in the final model.
FLUENT® requires that the velocity be given as a function (written in the C programming language) such that any value of velocity at any point on the boundary of interest may be determined. The U.D.F. is included below:

```
vprofile.c
UDF for specifying steady-state velocity profile boundary condition
************************************************************************/
#include "udf.h"

DEFINE_PROFILE(inlet_x_velocity, thread, position)
{
real x[ND_ND]; /* this will hold the position vector */
/*real z = 0;*/
face_t f;
  int i, n;
real R[31], V[31], v;
FILE *fp;
fp = fopen("RvsV_vectors.txt", "r");

n = 30; /*counter maximum*/
for (i=0; i<=n; i++)
{fscanf(fp, "%f%f", &R[i], &V[i]);

}

begin_f_loop(f, thread)
{
F_CENTROID(x,f,thread);
for (i=0; i<=(n-1); i++)
{
if (x[1]>=R[i] & x[1]<R[i+1])
```

```
{
v = V[i] + ((V[i+1]-V[i])/(R[i+1]-R[i]))*(x[1]-R[i]);

}
}
F_PROFILE(f, thread, position) = v;

}
end_f_loop(f, thread)
fclose(fp);
```

This U.D.F. initialises two arrays, one containing the node values in the range of the inlet, and the other the axial velocity magnitudes at these nodes. Because the nodes are close together, a simple linear interpolation between nodes was specified to smooth the function, such that:

$$v = \frac{\Delta v_{1-2}}{\Delta r_{1-2}} r + v_1 \tag{4.2}$$

Where v is the velocity, r is the radius, subscripts $1-2$ are the change between the consecutive known values, and subscript 1 is the previous known value.

Note on inlet velocity profile

It must be noted that due to the fact that the same velocities at inlet are used in spite of the inlet area changing, the volume flow rate will not be constant. However, it was expected that due to the extra constraints of the aorta at the inlet (see Section 3.2.2), the radial displacements of the ascending aorta would not cause an appreciable change in flow area. This was investigated and found to be the case (see Section 6.1), and the method was applied as described above.

Chapter 5

Interface and Coupling

This chapter explains the coupling process used in this investigation. The interface between the solid problem (in ABAQUS®) and the fluid problem (in FLUENT®) was written in the Matlab programming language and the code is included on the CD attached to this report. Principles upon which the the code was based, various algorithms used, and the purposes of each programme will be described in this chapter, preceeded by an introduction to the theory behind coupling.

5.1 What are coupled systems?

The aim of the investigation was to simulate the coupling between the solid and fluid problems in the ascending aorta. A coupled system is one consisting of at least two distinct systems, which overlap with common variables. Although each system is solved with a characteristic set of differential equations, the overlapping variables make it impossible to solve each system separately [5] and information has to be exchanged between the systems to fully solve the problem. Figure 5.1, shows the basics of a coupled system.

5.2 Coupling as applied to this study

The system in this investigation is the fluid structure interaction (FSI), and the common variables are displacement and pressure. The fluid problem is solved by the Navier-Stokes equations (see Section 2.2) and the solid probelm is solved for solid equilibrium (see Section 2.1). ABAQUS® and FLUENT® do not perform this coupling automatically.

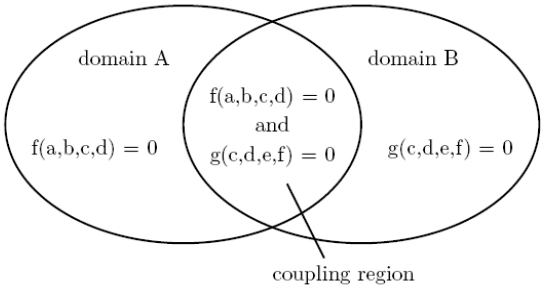

Figure 5.1: A coupled system showing two domains and a coupling region. Variables c and d are shared in the system. (courtesy of [5])

The fluid flow creates a pressure profile on the aortic wall, causing the structure to deform. The displacements of the solid boundary consequently cause a change in the flow, creating a new pressure profile, in turn changing the geometry of the boundary wall once again. In the steady flow scenario specific to this investigation, this continued to happen until an equilibrium was reached between the aortic wall and the blood flowing in the aorta.

The way the problem ran is as follows:

1. Blood flow was simulated and a pressure profile on the boundary was output.
2. The pressure profile was applied to the aortic wall outputting displacement values of the wall.
3. The new fluid domain boundary coordinates were aquired and a new flow domain defined.

The system repeated itself until equilibrium was reached.

5.2.1 Exchanged variables

The pressure profile required from the fluid system was that of total pressure at the common boundary, which is the sum of the static and dynamic pressures [45]:

$$\text{Total pressure} = \underbrace{\Delta p}_{static\ pressure} + \underbrace{\tfrac{1}{2}\rho v^2}_{dynamic\ pressure}$$

The deformations required from the solid system were the nodal displacements at the common boundary.

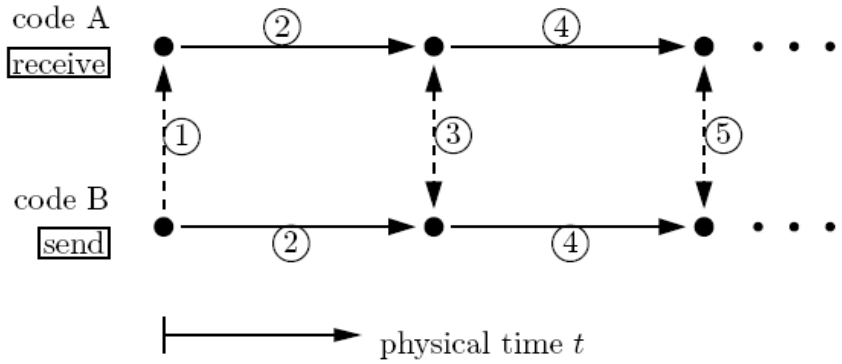

Figure 5.2: Initial exchange of data and subsequent parallel solving as used by MpCCI (courtesy of [5])

5.3 Available software for coupling problems

Mesh based Parallel Code Coupling Interface (MpCCI®) is a software designed to handle a range of coupling processes including the FSI as described in the above sections. MpCCI® searches the relevant input files for regions which exhibit coupling compatibility. This software uses a weak coupling system (that in which each system is solved separately) to solve the problem. MpCCI® runs a parallel solution that runs as shown in Figure 5.2.

The use of this software would have allowed a more complex model in this inves tigation as described in Section 1.2.

5.4 Sequence used for running the coupled simulation

The interface as created in this investigation minimised the requirement for manual data transfer as far as possible, however, in order to allow the process to be monitored and evaluated, the process was run in a series of steps. These steps are set out in the following flow chart (Figure 5.3) and each step is described in the following subsections of this chapter. For better clarity in the following sections, example files of the ABAQUS® input and data files as well as the FLUENT® case files have been included along with the programming code on the CD attached to this document.

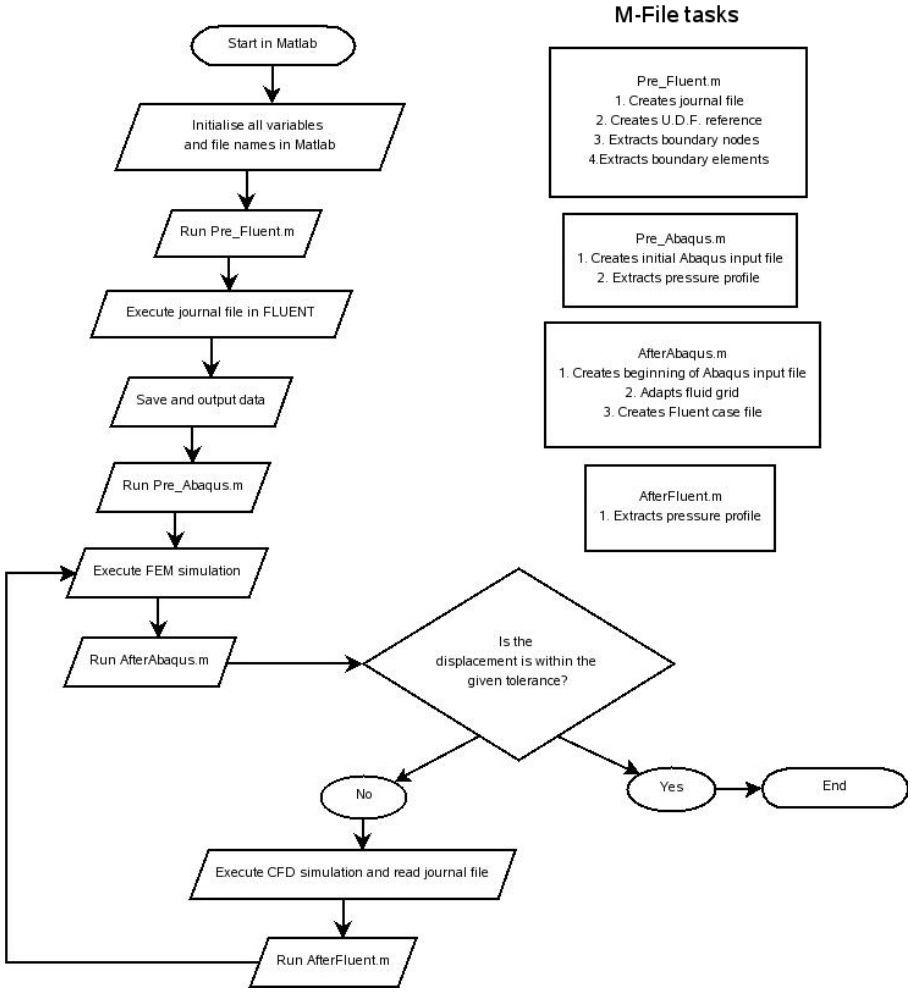

Figure 5.3: Flow chart showing the sequence of actions required to run a coupled simulation as defined in this investigation.

It should be noted, before describing any of the code, that when an axi-symmetric problem is specified in ABAQUS® , the Y-axis is the convention for the axis of symmetry, whereas FLUENT® uses the X-axis as the axis of symmetry. Therefore all coordinate systems were transformed accordingly.

5.4.1 Files required in working directory

For the simulation to run correctly, the following nine files needed to exist in the current working directory:

1. Pre_Fluent1.m
2. Initial FLUENT® case file, with the extension .cas
3. Pre_Abaqus1.m
4. Initial ABAQUS® input file, with the extension .inp. This file should not have a defined load and necessary changes as described in the corresponding section must be made.
5. AfterAbaqus.m with initial file names
6. AfterFluent.m
7. profile.c
8. journal_temp.txt
9. RvsVtemp.txt

5.4.2 Pre_Fluent1.m

Creation of journal file

This programme creates a journal file to be read by FLUENT® . A journal file (extension .jou) contains certain instructions which FLUENT® reads and executes. These commands are the same as those which can be typed directly into the FLUENT® console to perform the required actions. The journal file created by Pre_Fluent.m commands FLUENT® to extract the profile of total pressure and write it to a text file (extension .xy) which is given a standard name, and placed in the working directory.
The journal file is created from the template text file, named journal_temp.txt. The

additional information which Pre_Fluent1.m writes to the journal is the name of the pressure profile file to be created.

Creation of U.D.F reference file

The U.D.F. used for the velocity profile at the inlet to the aorta calls an array of the coordinates along the inlet boundary. Because it was expected that the range of the inlet would change and thus the array would have to be updated for U.D.F. to call the correct r values for each simulation. Pre_Fluent1.m creates the initial range for the U.D.F (profile.c) to read. The text file RvsVtemp.txt contains the template of initial coordinate values to be used.

Boundary node extraction

Because the nodes of interest are only those at the common boundary between fluid and solid, it was necessary to distinguish these from the rest of the nodes. A vector is created by Pre_Fluent1.m, which is then used by the subsequently run programmes, as the node numbering does not change, but the node coordinates corresponding to these numbers do.
This was acheived via a loop containing a condition forcing only the nodes along the common boundary to be placed into the vector. These nodes were then arranged in the ascending order of the node numbers.

Boundary element extraction

As an element set was defined in ABAQUS® for the inner wall of the aorta, these elements were listed in the input file (extension .inp) and were simply extracted and placed in a vector. In case of this element set not being defined in ABAQUS® , or if the input file is formatted without CAE (the user interface of ABAQUS®), a loop was created which can extract these elements on the condition that the nodes constituting the four element corners includes at least one of the node numbers in the boundary node vector as detailed in the above section.

5.4.3 Initial flow model case file

It was important that the same case file was used for all the models. The solver conditions may be altered but the grid formation (as created in GAMBIT®) had to come from the same file every time. The reason for this was that when a grid is created, the

bandwith of the solution matrix is optimised. Therefore, the nodes are numbered in an order specific to each model. The node connectivity as defined in the case file is written in a hexadecimal numbering system, which makes it complicated to analyse. It is consequently simpler to ensure that the same node numbering and thus the corresponding node connectivity is used for every model, to be compatible with the programming code creating the new case file for the subsequent job.

An unfortunate result of this is that the written code became very problem specific, and cannot be used generally for any rectangular grid created in GAMBIT® . Notwithstanding this, the code was written as generally as was possible.

5.4.4 Initial artery wall input file

This input file acts simply as a template for the first ABAQUS® simulation which is run. There is no defined loading, as the pressure profile created in FLUENT® acts as the initial loading condition. Various lines need to be added to this input file for it to output the correct information to the data file (extension .dat). Anywhere in the STEP section of the input file the following lines must be inserted:

```
*Node Print, Nset=Aorta-1.All, Freq=1
U1, U2, COORD
```

"*Node Print" specifies that information must be printed for the nodes specified in N-set. "Aorta-1" is the name of the part instance and "All" is the name of the set containing all the nodes of the part instance. "Freq" defines the frequency with which the information must be reported (i.e. it will be printed for every step if set to 1 as in the example).
The second line specifies the information that will be printed to the data file. "U1" and "U2" are the nodal displacements in the 1 and 2 directions respectively and "COORD" specifies that the original nodal coordinates are printed to the data file.

5.4.5 Pre_Abaqus1.m

By the time that this programme is run, the first FLUENT® simulation will have been completed. FLUENT® will have read the journal file and consequently created a text file containing the total pressure profile along the common boundary.

Creation of input file

The first job to be run by ABAQUS® needed to be created with the correct load applied to it. The first part of the programme extracts the formatted input file from the template file described in Section 5.4.4 and places it into a new file. The pressure profile is added to this input file by AfterAbaqus.m

Pressure profile extraction

The second task that Pre_Abaqus1.m performs is to extract the pressure profile from the text file created by FLUENT® . The profile is then placed into the correct format for ABAQUS® to read in a pressure using an analytical field, and acting on the boundary elements as isolated in the vector as previously described. As FLUENT® outputs nodal pressure values, and ABAQUS® applies pressures to the surfaces of elements, the average pressure between two nodes was applied to the element faces. For the initial pressure load on the artery wall, the change in systolic and diastolic pressure is added to the total pressure from the FLUENT® simulation.

5.4.6 AfterAbaqus.m

This programme is run after every ABAQUS® job has been completed. It requires the user to update the names of the files which are to be written to and read from. It is the only programme that needs to be altered after the initial setup. It also prints information to the screen which should be monitored by the user.

Creation of new input file

This programme extracts the information which was written to the data file (original coordinates, and displacement magnitudes). It sums the coordinates and displacements in each direction to get the new coordinates of the nodes. This new nodal information is written to a new input file, so that the next ABAQUS® job has the geometry of the previous job at completion. It also creates all the other sections of the new input file up until the loading section, which is only completed after FLUENT® has output the new pressure profile. The nodal displacements of the central boundary node are displayed to the screen, to enable the user to monitor the process.

Creation of new case file

AfterAbaqus.m copies all parts of the previous case file, except the nodal coordinates, into a new case file to be run in the next FLUENT® simulation. It also creates the new journal file to be read by FLUENT® so that the new pressure profile is written to a file. The new radius (y) coordinates at the inlet boundary are written to a file to be called by the U.D.F. for the new inlet velocity profile.

Grid adaptation

As the solid mesh geometry changes, the fluid grid must change accordingly. The boundary nodes are copied directly across from the ABAQUS® data file to the FLUENT® case file, using the vector of boundary node numbers, which was created in Pre_Fluent1.m, and placed into the correct positions in the new case file. However, to leave the rest of the grid as it was for the previous job would yield unreliable results and render all refinements in the initial grid futile (see Section 4.2). Therefore it was required that the grid be adapted to the new geometry of the wall boundary, and it was chosen to acheive this by the method set out below:

The axial coordinates were simply stacked one below the other, that is the nodes lay on lines perpendicular to the axis of symmetry. Therefore, all X-coordinates of equal value in the initial simulation, had equal values in all subsequent runs.
The Y-coordinates (those parallel to the radial axis) were interpolated such that:

$$\frac{y_{2f} - y_{1f}}{y_{bf} - y_{sf}} = \frac{y_{2i} - y_{1i}}{y_{bi} - y_{si}} \tag{5.1}$$

where subscripts f and i are the new grid values and old grid values respectively, 1 and 2 are any two consecutive nodes and b and s are the nodes at the boundary and axis of symmetry respectively. In this way, the refinements near the artery wall are not lost or meaningless.

5.4.7 AfterFluent.m

This programme is run after the second FLUENT® simulation, and after all FLUENT® simulations for the rest of the process. It's only task is to extract the pressure profile created by FLUENT® according to the instructions in the journal file and append it, along with the remainder of the input file, to the incomplete ABAQUS® input file,

created by AfterAbaqus.m. The total pressure is applied without the addition of the change between systolic and diastolic pressures.

5.5 Conditions for convergence

The process was expected to reach a steady state at which point the displacements of the aortic wall become equal for each iteration. The difference between the subsequent displacement values was monitored until it was satisfied that:

$$\frac{d^{i+1} - d^i}{d^i} \leq \text{tolerance} \tag{5.2}$$

where tolerance $= 9.5 \times 10^{-8}$ A number of subsequent iterations were run after this point to ensure that no further fluctuations would occur.

Chapter 6

Results and Discussion

The models were first run independently and later coupled. The current chapter will first provide the details of the independent wall model simulations and a short discussion of these results.
The independent blood flow model results will then be presented and discussed, starting with the results of the inlet velocity profile investigation as detailed in section 4.6 and followed by the final fluid model as modelled on this data.
The results of the coupled models will then be presented and discussed and finally a comparative discussion on the independent and coupled models will be given.

6.1 Independent wall models

For the artery wall models the focus of the results was on principal stresses and strains, as well as those in the axial and radial directions. Compliance calculations were for the maximum, minimum and averaged values.

Single layer models were formed by the averaging of the medial and adventitial layer material properties, according to their area (see Section 3.2.6). Two layer models comprised of a layer of medial material and a layer of adventitial material in the healthy aorta models as discussed in Section 3.2.6.

The independent wall models were loaded with the difference in pressure magnitudes between the systolic and diastolic phases of the heart, as described in Section 3.2.3. Compliance was calculated as described in Equation 3.9 and is a measure of the change of the diameter of an artery with pressure loading.

6.1.1 Independent single layer, isotropic model

The values for this model are set out in Tables 6.1, 6.2 and 6.3 and contour plots of the principal stresses and strains are displayed in Figures 6.1 and 6.2.

	Compliance (%100mmHg)
Max	24.5228
Min	15.7448
Ave	22.3544

Table 6.1: Maximum, minimum and average compliance values for independent, single layer, isotropic ascending aorta

Principal Stress	Max compressive stress	3.1148E-04
(MPa)	Max tensile stress	5.0903E-03
Radial Stress	Max compressive stress	6.2523E-03
(MPa)	Max tensile stress	–
Axial Stress	Max compressive stress	6.2523E-03
(MPa)	Max tensile stress	3.8523E-03

Table 6.2: Maximum principal, radial and axial stresses in independent single layer, isotropic ascending aorta model

Principal Strain	Max compressive	–
-	Max tensile	0.0961
E11	Max compressive	0.1202
-	Max tensile	–
E22	Max compressive	0.0168
-	Max tensile	0.0509

Table 6.3: Maximum principal, radial and axial stresses in independent, single layer, isotropic ascending aorta model

6.1.2 Independent two layer, isotropic model

The values for this model are set out in Tables 6.4, 6.5 and 6.6, and contour plots of the principal stresses and strains are displayed in Figures 6.3 and 6.4.

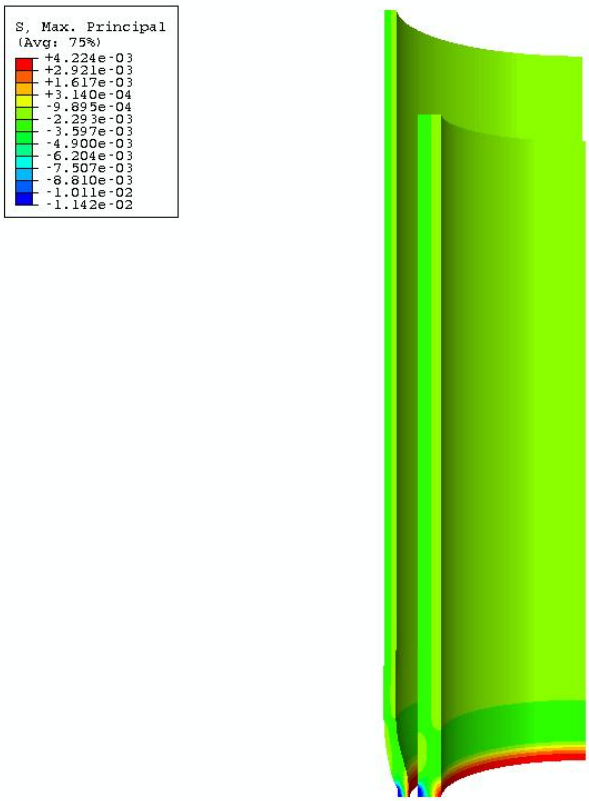

Figure 6.1: Principal stress for the independent isotropic, single layer model, with a deformation scale of 3

	Compliance (%100mmHg)
Max	24.4606
Min	15.6577
Ave	22.3622

Table 6.4: Maximum, minimum and average compliance values for independent, two layer, isotropic ascending aorta

Principal Stress	Max compressive stress	1.9724E-03
(MPa)	Max tensile stress	6.6309E-03
Radial Stress	Max compressive stress	6.1829E-03
(MPa)	Max tensile stress	–
Axial Stress	Max compressive stress	4.5451E-03
(MPa)	Max tensile stress	4.9148E-03

Table 6.5: Maximum principal, radial and axial stresses in independent two layer, isotropic ascending aorta model

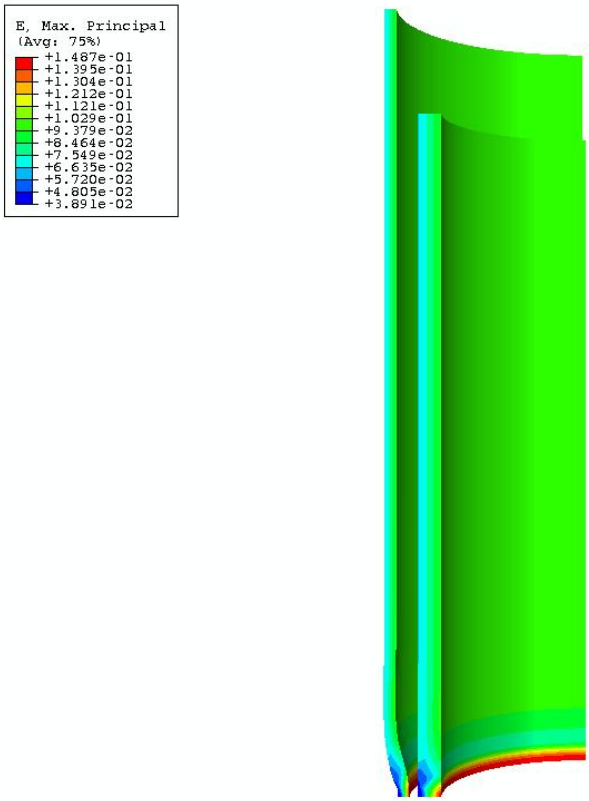

Figure 6.2: Principal strain for the independent isotropic, single layer model, with a deformation scale of 3

Principal Strain	Max compressive	–
-	Max tensile	0.0960
E11	Max compressive	0.1145
-	Max tensile	–
E22	Max compressive	0.1145
-	Max tensile	0.0478

Table 6.6: Maximum principal, radial and axial stresses in independent, two layer, isotropic ascending aorta model

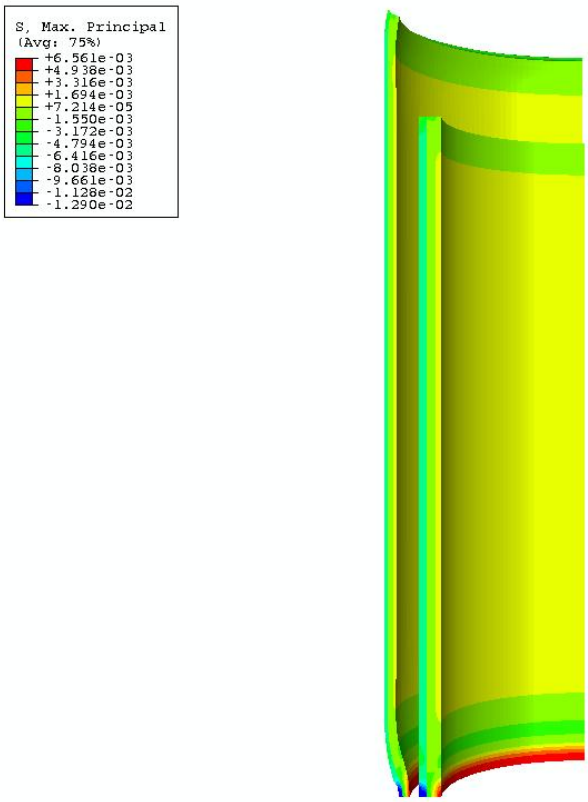

Figure 6.3: Principal stress for the independent isotropic, two layer model, with a deformation scale of 3

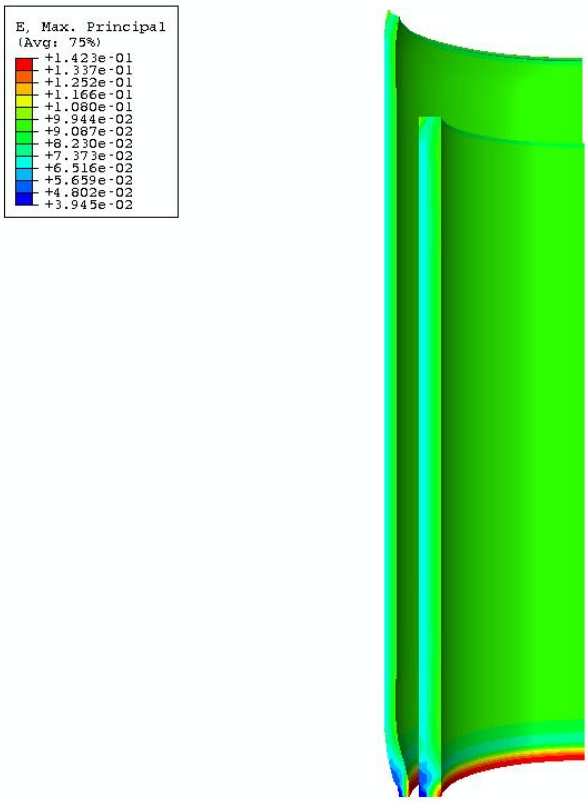

Figure 6.4: Principal strain for the independent isotropic, two layer model, with a deformation scale of 3

6.1.3 Independent two layer, orthotropic model

The values for this model are set out in the Tables 6.7, 6.8 and 6.9, and contour plots of the principal stresses and strains are displayed in Figures 6.5 and 6.6.

	Compliance (%100mmHg)
Max	27.1784
Min	17.1680
Ave	24.8793

Table 6.7: Maximum, minimum and average compliance values for independent, two layer, orthotropic ascending aorta

Principal Stress	Max compressive stress	5.2073E-03
(MPa)	Max tensile stress	8.3529E-03
Radial Stress	Max compressive stress	6.6637E-03
(MPa)	Max tensile stress	–
Axial Stress	Max compressive stress	5.2078E-03
(MPa)	Max tensile stress	6.0144E-03

Table 6.8: Maximum principal, radial and axial stresses in independent two layer, orthotropic ascending aorta model

Principal Strain	Max compressive	–
-	Max tensile	0.1067
E11	Max compressive	0.1208
-	Max tensile	–
E22	Max compressive	0.0254
-	Max tensile	0.0491

Table 6.9: Maximum principal, radial and axial stresses in independent, two layer, orthotropic ascending aorta model

6.1.4 Aged aorta model

It can be seen immediately from the visualisation (Figures 6.7, 6.8 and 6.9) of the three diseased aorta models under a constant pressure load that the results are not accurate. Therefore this model was not included in a coupled process.

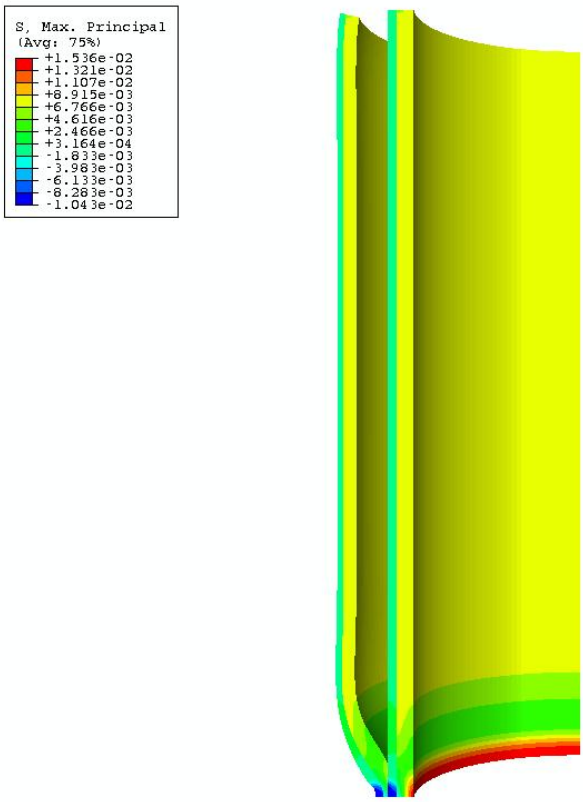

Figure 6.5: Principal stress for the independent orthotropic, two layer model, with a deformation scale of 3

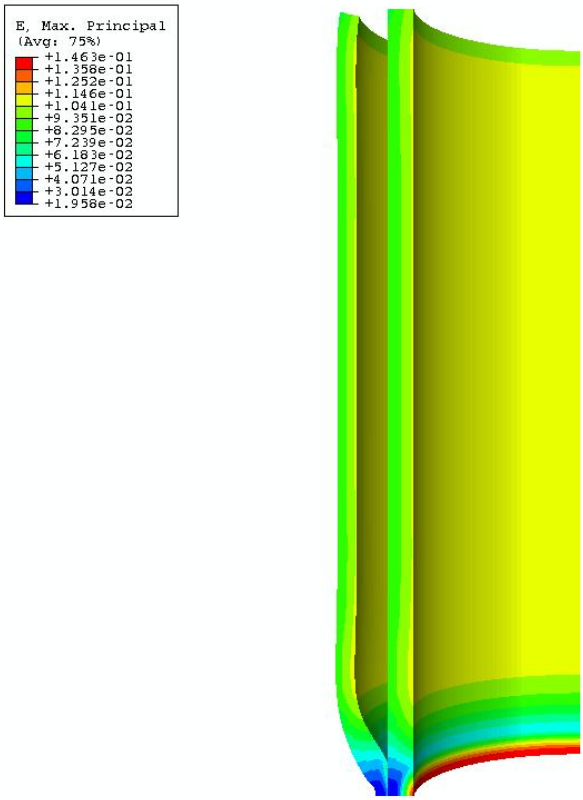

Figure 6.6: Principal strain for the independent orthotropic, two layer model, with a deformation scale of 3

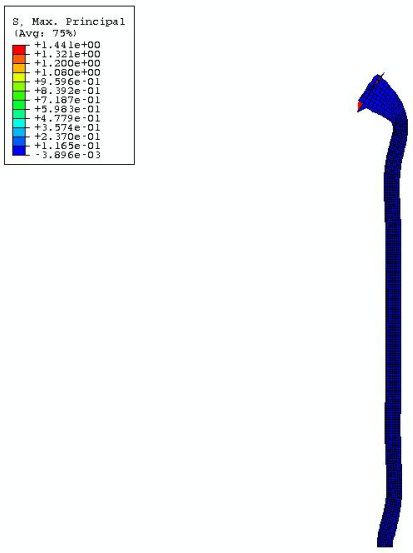

Figure 6.7: Resulting geometry of arteriosclerosis with a 0.2mm intima layer

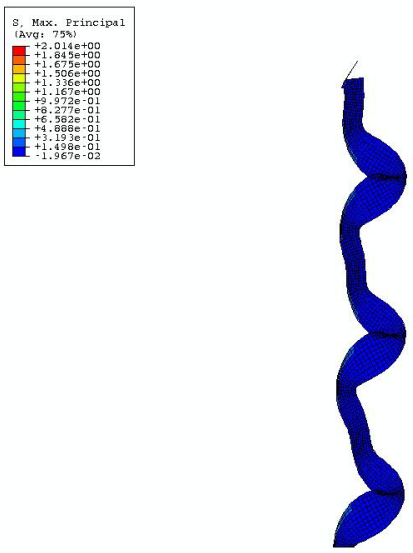

Figure 6.8: Resulting geometry of arteriosclerosis with a 0.4mm intima layer

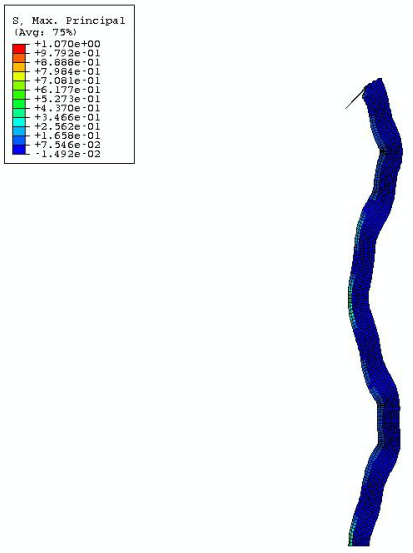

Figure 6.9: Resulting geometry of arteriosclerosis with a 0.6mm intima layer

6.1.5 Discussion of the independent wall models

The data shows a maximum compressive principal stress value existing in the two layer, orthotropic model, with a value of $5.21 \times 10^{-3} MPa$. The tensile value was also highest in this model, with a value of $8.3529 \times 10^{-3} MPa$. The tensile stress values get higher with the complexity of the model.
This effect is likely to be due to the different material properties of the layers non-linearising the elastic properties.

None of the models experienced any tensile stresses or strains in the radial direction, but this due to the particular loading of the specimen. In the axial direction there was some tensile stress, which may be due to the "stretching" of the specimen to compensate for the expansion under the inlet and outlet constraints.

The maximum compliance was greatest in the two layer, orthotropic model and the differences in maximum and minumum values for all of the models were within 10% of each other. The lower compliance values are due to the constraints around the aorta at the inlet, preventing expansion at this point. The minimum values are not entirely relevant, as the constraints act as a counter-pressure, and thus the applied pressure is not a sensible value.

6.2 Independant blood flow models

6.2.1 Results of investigation into inlet velocity profile

As discussed in Section 4.6 a relatively flat velocity profile was expected. The investigation yeilded a profile in accordance with this expectation as shown in Figure 6.10.

At the nodes just in from the wall, the velocity magnitude was approximately $4.62 \times 10^3 m/s$, which is 7.84% of the average value.
The velocity magnitude did not reach a peak value on the axis of symmetry, but rather dipped slightly in the this region. The maximum velocity value occured at a radius of $10.36mm$, and was $12.06 \times 10^2 m/s$. At the centre of the aorta the velocity was equal to $99.15 \times 10^2 m/s$.

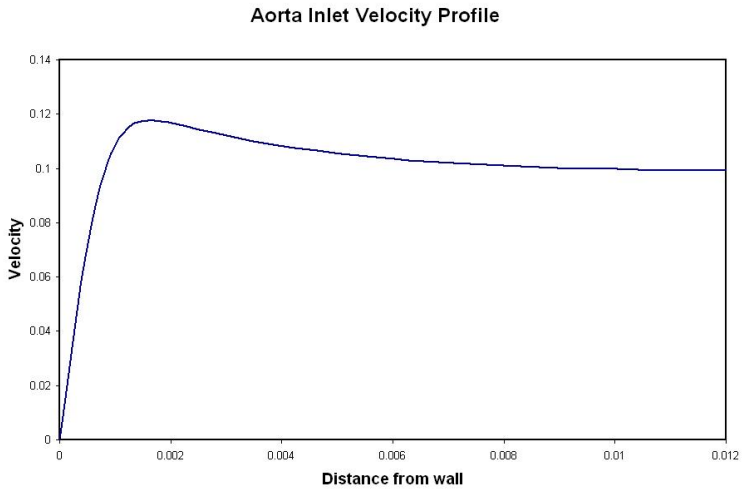

Figure 6.10: Inlet velocity profile for half the diameter of the aorta resulting from investigation

6.2.2 Final blood flow model

The flow in the ascending aorta did not reach a fully developed state which can be seen from Figure 6.11.

The total pressure at the wall had a maximum value of $1.044 \times 10^{-5} MPa$, and a minimum value of $1.409 \times 10^{-5} MPa$. These are the results for the first iteration of the coupled jobs as no input data was required from ABAQUS® .

The pressure profile obtained from this intial flow model is the first pressure defined in the ABAQUS® input file. The profile in Figure 6.12 shows only the total pressure, before it is added to the change in pressure from diastole to systole ($40 mm$Hg).

The exit velocity profile for fully developed laminar flow would be parabolic, but this was not the case at the exit to the aorta model as shown in Figure 6.13.

6.3 Coupled wall/blood flow models

The coupled simulations were run until the system reached a steady state. This state was reached when the condition specified in Equation 5.2 was satisfied.

As the first pressure profile on the wall included the change in pressure from diastole to systole, the displacement value was not comparable with the subsequent displacement

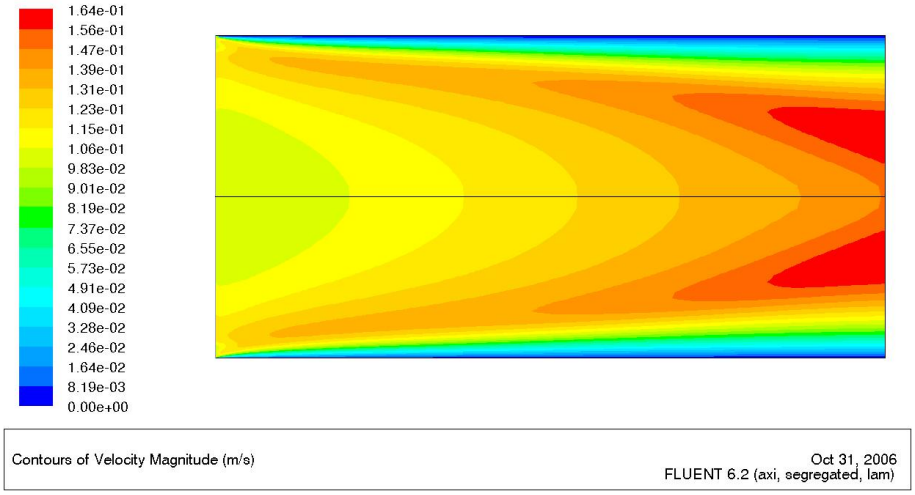

Figure 6.11: Velocity contours resulting from initial flow model

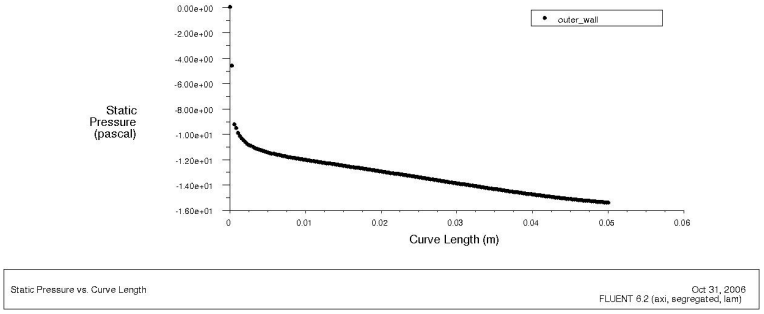

Figure 6.12: Pressure profile output from initial CFD simulation

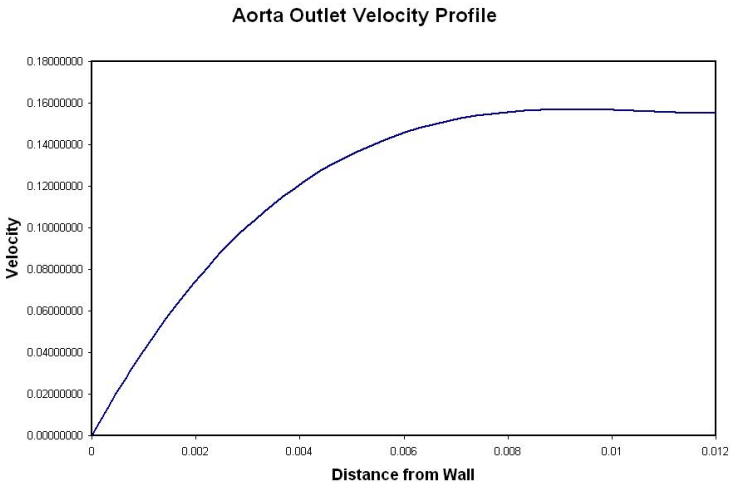

Figure 6.13: Outlet velocity profile for half the diameter of the ascending aorta

values and was this initial iteration is not shown in the relevant graphs in the following sections. The same blood flow model was used for all of the wall models. The size of the displacement of the central boundary node for each iteration was compared with that for the previous iteration, and the difference in these values is shown in the graphs displayed for each section.

6.3.1 Coupled single layer, isotropic model

The difference between subsequent displacement sizes of the central boundary node are shown in Figures 6.14 and 6.15.

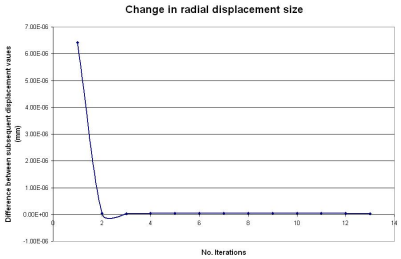

Figure 6.14: Graph showing convergence process for radial displacements in the isotropic, single layer model

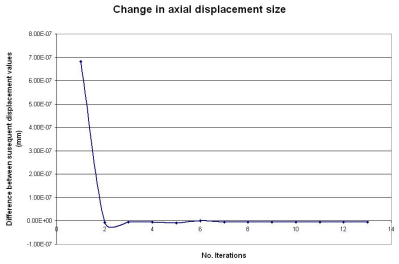

Figure 6.15: Graph showing convergence process for axial displacements in the isotropic, single layer model

The results for this model are shown in the tables below:

	Compliance (%/100mmHg)
Max	25.1134
Min	3.5858
Ave	21.6846

Table 6.10: Maximum, minimum and average compliance values for coupled, single layer, isotropic ascending aorta

6.3.2 Coupled two layer, isotropic model

The difference between subsequent displacement sizes of the central boundary node are shown in Figures 6.16 and 6.17.

The results for this model are shown in the Tables 6.13, 6.13 and 6.15.

Principal Stress	Max compressive stress	1.0700E-03
(MPa)	Max tensile stress	1.1886E-02
S11	Max compressive stress	5.2820E-03
(MPa)	Max tensile stress	4.9920E-03
S22	Max compressive stress	1.2464E-02
(MPa)	Max tensile stress	1.1862E-02

Table 6.11: Maximum principal, radial and axial stresses in coupled single layer, isotropic ascending aorta model

Principal Strain	Max compressive	–
-	Max tensile	0.1152
E11	Max compressive	0.1076
-	Max tensile	0.0903
E22	Max compressive	0.1296
-	Max tensile	0.1148

Table 6.12: Maximum principal, radial and axial stresses in coupled, single layer, isotropic ascending aorta model

	Compliance (%/100mmHg)
Max	25.2184
Min	1.3567
Ave	21.6203

Table 6.13: Maximum, minimum and average compliance values for coupled, two layer, isotropic ascending aorta

Principal Stress	Max compressive stress	1.2920E-03
(MPa)	Max tensile stress	1.5357E-02
S11	Max compressive stress	5.2830E-03
(MPa)	Max tensile stress	4.8740E-03
S22	Max compressive stress	1.0601E-02
(MPa)	Max tensile stress	1.5317E-02

Table 6.14: Maximum principal, radial and axial stresses in coupled two layer, isotropic ascending aorta model

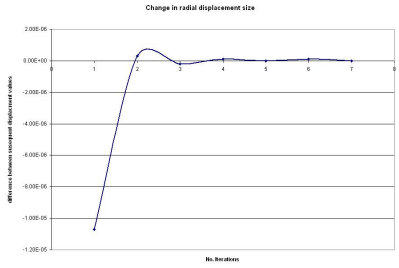

Figure 6.16: Graph showing convergence process for radial displacements for the isotropic, two layer model

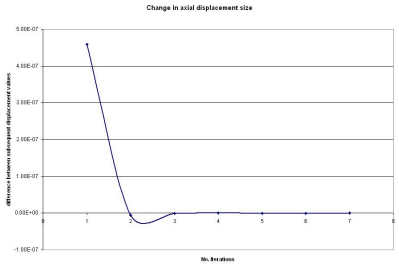

Figure 6.17: Graph showing convergence process for axial displacements for the isotropic, two layer model

Principal Strain	Max compressive	–
-	Max tensile	0.1315
E11	Max compressive	0.1182
-	Max tensile	0.1177
E22	Max compressive	0.1600
-	Max tensile	0.1308

Table 6.15: Maximum principal, radial and axial stresses in Coupled, two layer, isotropic ascending aorta model

6.3.3 Coupled two layer, orthotropic model

The difference between subsequent displacement sizes of the central boundary node are shown in Figures 6.18 and 6.19.

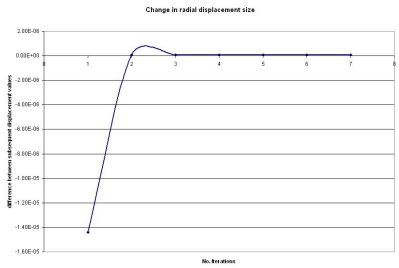

Figure 6.18: Graph showing convergence process for radial displacements for the orthotropic, two layer model

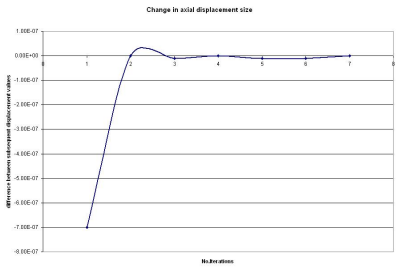

Figure 6.19: Graph showing convergence process for axial displacements for the orthotropic, two layer model

The results for this model are shown in the Tables 6.16, 6.17 and 6.18 and contour plots of the maximum principal stresses and strains are displayed in Figures 6.20 and 6.21

	Compliance (%/100mmHg)
Max	27.9850
Min	2.0297
Ave	24.0727

Table 6.16: Maximum, minimum and average compliance values for coupled, two layer, orthotropic ascending aorta

Principal Stress	Max compressive stress	1.6540E-03
(MPa)	Max tensile stress	1.7193E-02
S11	Max compressive stress	5.2750E-03
(MPa)	Max tensile stress	4.8510E-03
S22	Max compressive stress	1.1142E-02
(MPa)	Max tensile stress	1.7161E-02

Table 6.17: Maximum principal, radial and axial stresses in coupled two layer, orthotropic ascending aorta model

Principal Strain	Max compressive	–
-	Max tensile	0.1351
E11	Max compressive	0.1251
-	Max tensile	0.1199
E22	Max compressive	0.1665
-	Max tensile	0.1347

Table 6.18: Maximum principal, radial and axial stresses in coupled, two layer, orthotropic ascending aorta model

The final flow domain for the orthotropic, two layer model is shown in Figure 6.22 to illustrate the adapted grid as outlined in Chapter 5. Figure 6.3.3 shows the velocity contours resulting from this grid.

The pressure profile alters due to the different grid geometry as shown in Figure 6.23, which is the final pressure profile applied to the ABAQUS® model in the coupled orthotropic, two layer model.

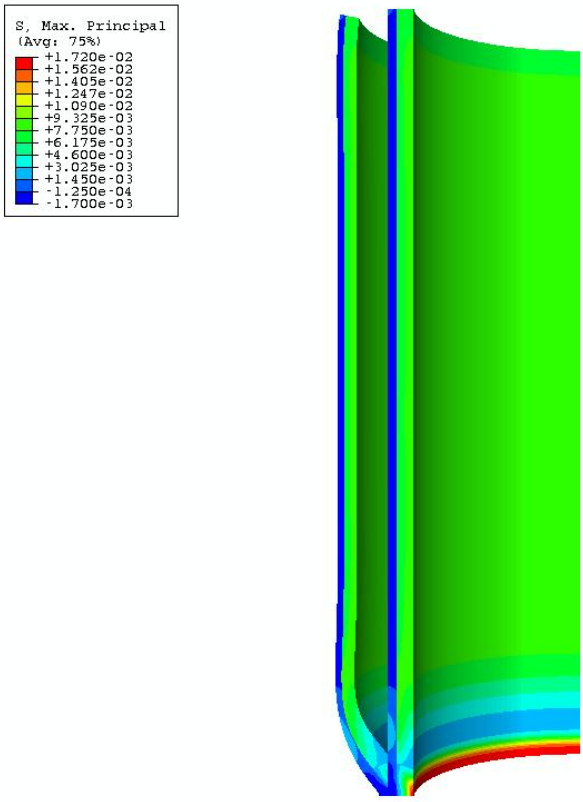

Figure 6.20: Principal stress for the coupled orthotropic, two layer model for the first iteration, with a deformation scale of 3

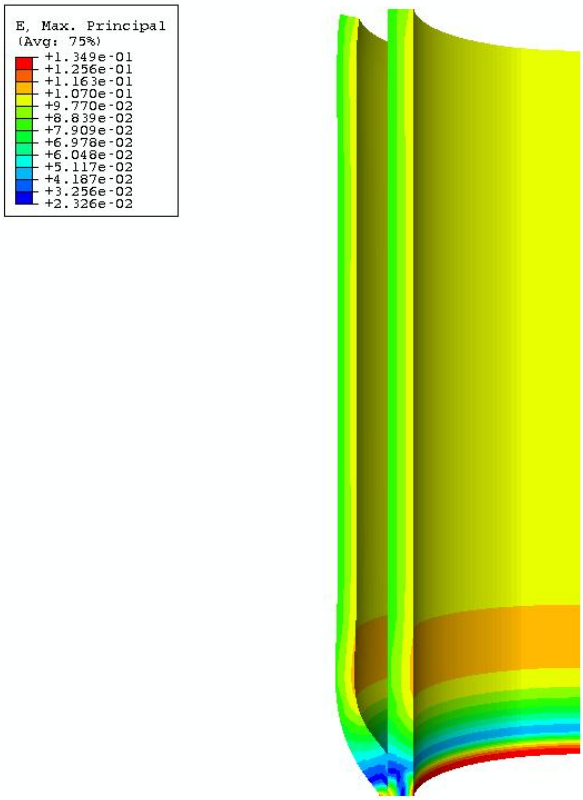

Figure 6.21: Principal strain for the coupled orthotropic, two layer model for the first iteration, with a deformation scale of 3

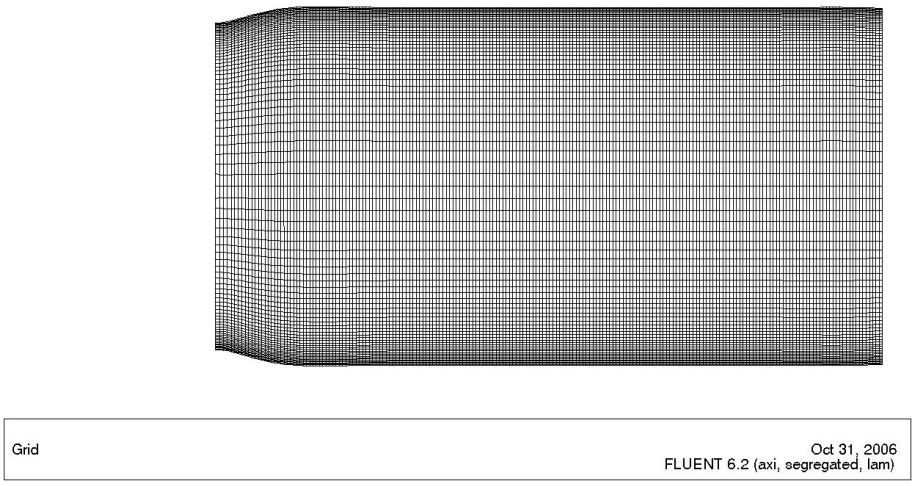

Figure 6.22: The adapted mesh for the final orthotropic, two layer flow domain

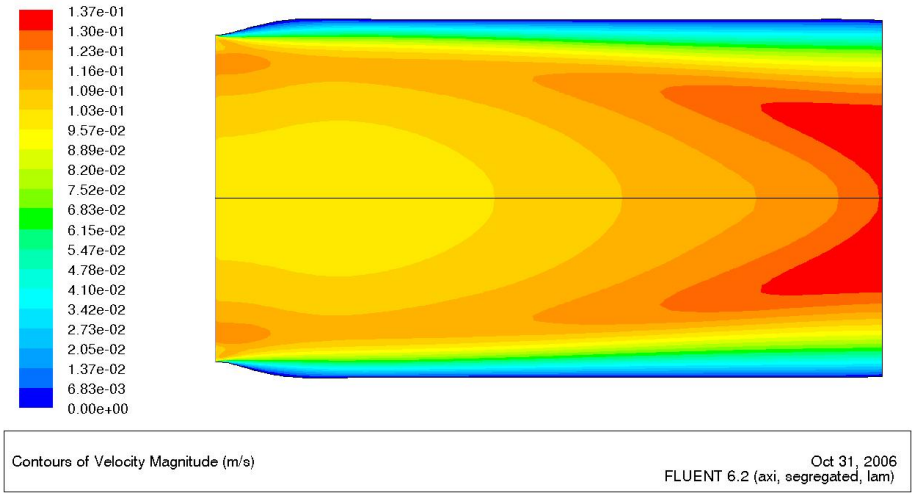

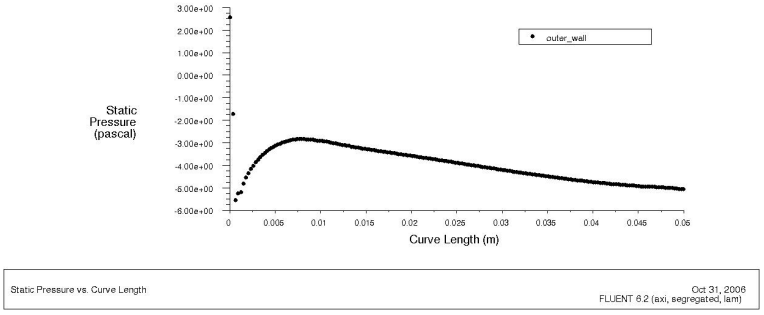

Figure 6.23: Pressure profile reulting from final CFD simulation in the orthotropic, two layer model

6.3.4 Discussion of coupled results

As in the independant models the greatest maximum principal stress result occured in the orthotropic, two layer model, with a value of $1.65 \times 10^{-3} MPa$ for the compressive stress and $1.72 \times 10^{-2} MPa$ for the tensile stress. Again the values increased with the complexity of the model.

As before the maximum compliance value occurred in the orthotropic two layer model, with a value of 27.99%. The minimum compliance values were all less than 5%, but these values occurred close to the inlet and may be attributed to the constraints in this region.

6.4 Discussion and comparison of results

6.4.1 Stress and strain values

The maximum compressive principal stress value was $5.2073 \times 10^{-3} MPa$ and occured in the orthotropic, two layer independent model, while the minimum value was $3.1148 \times 10^{-4} MPa$ and occurred in the independent isotropic, single layer model. The fact that these extremes occured in the independent models shows that the pressure profile from the blood flow may have a smoothing effect on the stresses occurring in the walls. The pressure drop may also account for lowered stresses in the coupled models.

The maximum principal strain value occured in the coup led orthotropic, two layer model, with a value of $0.1351 MPa$. The strain values for the independent models were all within $0.0107 MPa$ of each other, and those for the coupled models were within $0.0199 MPa$ of each other and all of the strains were tensile.

The principal stresses and strains were generally larger for the coupled models, but this may be attributed to the fact that a differential pressure added for each iteration, effectively building on to the initial pressure. Where this is not the case, is likely to be due to the pressure drop, through the flow domain, lowering the overall value of the pressure.
Also, the non-linearity of the pressure profile is likely to cause the aorta to deform non-uniformly. The uneven deformations resulting from this may “pull” the material in different directions, increasing the tension through the vessel. This may also have been the cause of the radial tensile stresses and strains occuring in the coupled models in that as the pressure profile becomes uneven, the load is no longer fully compressive.

It is apparent that the high stress regions are generally in the constrained sections of the models. These sections include the inlet constraint, where the vessel has a concentrated stress region over the supported inlet region, and the outlet condition, where the interaction seems to be pulling the aorta, preventing the deformations.

The radial stresses were mainly compressive, which is expected as there is an expansion in the direction of the force, while the axial stresses are mainly tensile, due to the stretching of the aorta because of the outlet condition.

6.4.2 Compliance values

The compliance in the models ranged between minimum values of 1.36% and 17.1 7% ,and maximum values of 24.46% and 27.99%. The minimum values were due to the small displacements in the inlet region, where the constraints prevent them from having larger values. The fact that there is essentially a pressure opposing the movement makes this small compliance value irrelevant.

The average compliance values for the coupled jobs differed from those for the independent models by 0.67% for the isotropic single layer model, 0.74% for the isotropic two layer model and 0.81% for the orthotropic two layer model. The average values for the all of the independent models were higher, but this is due to the low minimum values. The maximum compliance value for every independent model is lower than that of its corresponding coupled model, therefore it is safe to say that the effect of the blood flow on the aorta was to increase the compliance.

The compliance values (both the average and maximum values) are within the range for physiological values with the two layer, orthotropic model yielding the greatest compliance value of 27.99%, as compared to the lowest maximum value, occuring in the isotropic, two layer model, of 24.46%.

6.4.3 Mesh refinements

It was important that a finer mesh would not yield substantially different results. Therefore the initial, independent wall jobs were run with a refined mesh. The difference in results obtained were unsubstantial and therefore the mesh was not altered.

Chapter 7

Conclusions and Recommendations

7.1 Consistency of results

The resulting maximum and average compliance values in the investigation of a young and healthy were all well within the physiological range. The minimum values were lower than those in physiological data, but this is due to the particular constraints around these regions (those close to the aorta inlet) and therefore does not negate the relevance of the other data.
The stress and strain values in the investigation may be seen as verified as they have a direct relationship with the displacement and pressure values resulting in the compliance. The range of physiological data is very large, so there is room for very different results to exist and therefore the data aquired in this investigation should not be seen as conclusive.

The suspicious results yielded in the diseased aortic model should be investigated, as they are not consistent with the results from the other models. The effects of such drastic geometrical changes in an ascending aorta on blood flow should also be investigated, in case of there being a reasonable cause for results of this nature.

7.2 Relevance of investigation

The realistic values obtained as discussed in the previous section and their consistency with the uncoupled simulations show that the coupling process used was effective.

7.3 Linear elasticity and steady flow

The non-linearity of artery walls has a smoothing effect on the pressure waves in the arterial system. One of the effects of this is the effective pushing of blood onward through the arteries, releasing strain on the heart. If the blood flow in the models had been modelled as pulsatile, the linear elastic artery would not have shown any of this effect. Also, if the artery elasticity were modelled as non-linear, while the blood flow were transient, the reality of the interaction would again not be fully captured.

7.4 The limitations of axi-symmetric modelling

The axi-symmetric nature of the model was directly associated with the appriximation of the ascending aorta being a straight cylinder. The irregularity of the aorta geometry may cause a number of interesting effects on the blood flow that cannot be captured by an axisymmetric modelling process and an investigation into this would be of great value.

7.5 Further developments to the artery wall models

A bottom up engineering approach was used in this investigation, and there are many extensions which could be implemented. The effects of visco-elasticity should be analysed, possibly starting with a hyper-elastic model to investigate the non-linearity of the mechanical properties with increased loading.
As previously discussed, the effects of a three dimensional geometry should be included in subsequent studies.

7.6 Further developments to the blood flow models

The blood flow in this study was not pulsatile. The true nature of blood flow and its effects on the artery walls requires a fully transient model, especially with regard to the stresses induced in the artery walls.

7.7 Further developments to the coupling method

The static nature of the simulations in ABAQUS® and FLUENT® forced the superposition of resulting values, this may have led to a certain amount of error in the results. A coupling procedure that allows a dynamic analysis process to be carried out would be of great value here, and the use of an investigation, either using existing software (for example MpCCI®) or the creation of an extended interfacing code (such as that created for the purpose of this study) is highly recommended.

References

[1] F.H. Netter. *Interactive Atlas of Human Anatomy*. Novartis, Summit, USA (NJ), 1998.

[2] Lung National Heart, Blood Institute: Diseases, and conditions index: How the heart works. `http://www.nhlbi.nih.gov/health/dci/Diseases/Hf/HF_HowHeartWorks.html`. last accessed: October 2006.

[3] G.A. Holzapfel. A new constitutive framework for arterial wall mechanics and a comparative study of material models. *Journal of elasticity*, 61(8), November 2000.

[4] A. Herrmann. Numerical modelling of cardiovascular prostheses incorporating nitinol structure. Master's thesis, Cardiovascular Research Unit, University of Cape Town, 2005.

[5] *MpCCI Documentation*.

[6] Y.C. Fung. *Biomechanics: Mechanical properties of living tissues*. Springer-Verlag, New York, 2nd edition, 1993.

[7] Thorsten Koch. Non-linear finite element analyses of the aortic heart valve. Master's thesis, Department of Mathematics and Applied Mathematics, University of Cape Town, September 2004.

[8] Janoske, Silber, Kroger, Stanull, Benderoth, Schmitz-Rixen, Vogl, and Moosdorf. Fluid-structure interaction in abdominal aortic aneurysms. *Journal of Biomechanics*, 127(775), 2005.

[9] R.D. Cook. *Finite element modelling for stress analysis*. John Wiley and Sons, Inc., 1995.

[10] H.K. Versteeg and W. Malalasekera. *An Introduction to Computational Fluid Dynamics, the Finite Volume Method*. Pearson Prentice Hall, 1995.

[11] Robert E. Shadwick. Mechanical design in arteries. *The Journal of Experimental Biology*, 202(23):3305–13, 1999.

[12] Karl Perktold and Gerhard Rappitsch. Computer simulation of local blood flow and vessel mechanics in a compliant carotid artery bifurcation model. *J. Biomechanics*, 28(7):845–856, 1995.

[13] K. Perktold, R.O. Peter, M. Resch, and G. Langs. Pulsatile non-newtonian flow characteristics in three-dimensional carotid bifurctaion models: numerical study of flow phenomena under different bifurcation angle. *Journal of Biomedical Engineering*, 13:507–515, 1991.

[14] K. Perktold and G. Rappitsch. Mathematical modelling of local arterial flow and vessel mechanics. *Computational Methods for Fluid-Structure Interaction*, 1994.

[15] H.P. Osenberg. Simulation des arteriellen bluflusses- ein allgemeines modell mit anwendung auf das menschliche hiringefäbsystem. *ETH-Zürich*, 9342.

[16] Feng Gao, Masahiro Watanabe, and Teruo Matsuzawa. Stress analysis in a layered aortic arch model under pulsatile blood flow. *BioMedical Engineering Online*, 5(25), April 2006.

[17] G. Pedrizzetti et al. Pulsatile flow in moderately elastic arteries, its modelling and effects on elasticity. *Comuter Methods in Biomechanics and Biomedical Engineering*, 5(3):219–231, 2002.

[18] *Abaqus Theory Manual*.

[19] *Fluent Theory Manual*.

[20] Y. Papaharilaou, D.J. Doorly, and S.J. Sherwin. The influence of out-of-plane geometry on pulsatile flow within a distal end-to-side anastomosis. *J. Biomech*, 35:1225–1239, 2002.

[21] J.G Myers, J.A. Moore, M. Ojha, K.W. Johnston, and C.R. Ethier. Factors influencin blood flow patterns in the human right coronary artery. *Ann. Biomed. Eng.*, 29:109–120, 2001.

[22] B. Berthier, R. Bouzerar, and C. Legallais. Blood flow patterns in an anatomically realistic coronary vessel: influence of three different reconstruction methods. *J. Biomech*, 35:1347–1356, 2002.

[23] T. Naruse and K. Tanishita. Large curvature effect on pulsatile entrance flow in a curved tube: model experiment simulating blood flow in aortic arch. *J. Biomech Eng.*, 118:180–186, 1996.

[24] L. Morris, P. Delassus, A. Callanan, M. Walsh, F. Wallis, P. Grace, and T. McGloughlin. 3-d numerical simulation of blood flow through models of the human aorta. *Journal of Biomechanical Engineering*, 127:767–774, October 2005.

[25] N. Shahcheragi, H.A. Dwyer, A.Y. Cheer, A.I.Barakat, and T. Rutaganira. Unsteady and three dimensional simulation of blood flow in the human aortic arch. *J. Biomech Eng.*, 124:378–387, 2002.

[26] N. Engel. Abdominal aortic aneurysm and low back pain. *Dynamic Chiropractic*, 14(16), 1996.

[27] W.F. Ganong. *Review of Medical Physiology.* Lange Medical Publications, 1963.

[28] C.A. Schulze-Bauer, C. Morth, and G.A. Holzapfel. Passive biaxial response of aged human iliac arteries. *Journal of Biomechanical Engineering*, 125:395–496, 2003.

[29] Glossary of Terms for the Institute for Non-Newtonian Fluid Mechanics Mechanics Institute for Non-Newtonian Fluid. `http://innfm.swan.ac.uk/innfm/updated/content/about/glossary`. last accessed: October 2006.

[30] Gerhard A. Holzapfel. Determination of material models for arterial walls from uniaxial extension tests and histological structure. *Journal of Theoretical Biology*, May 2005.

[31] W. von Maltzahn, R.G. Warriyar, and W.F. Keitzer. Experimental measurements of elastic properties of media and adventitia of bovine carotid arteries. *Journal of Biomechanics*, 17:839–847, 1984.

[32] University of Cape Town members Cardiovascular Research Unit. Private communication, 2006.

[33] T. Koch and T. Franz. Review of properties of native human aorta at different sites. Technical report, Cardiovascular Research Unit, University of Cape Town, 2006.

[34] M.K. Erol, M. Yilmaz, Y. Oztasyonar, S. Sevimli, and H. Senocak. Aortic distensibility is increasing in athletes. *Am J Cardiol*, 89(8):1002–4, 2002.

[35] K. Hirata, F. Triposkiadis, E. Sparks, J. Bowen, C.F. Wooley, and H. Boudoulas. The marfan syndrome, abnormal aortic elastic properties. *J Am Coll Cardiol*, 18(1):57–63, 1991.

[36] Y.C. Fung. *Biomechanics Circulation*. Springer, New York, 2nd edition, 1997.

[37] J.D. Hart. *Nonparametric Smoothing and Lack-of-Fit Tests*. Springer-Verlag New York Inc, first edition, 1997.

[38] R.M. Nerem, W.A. Seed, and N.B. Wood. An experimental study of the velocity distribution and transition to turbulence in the aorta. *Journal of Fluid Mechanics*, 52:137–160, 1972.

[39] W. Nichols and M.F. Rourke. *McDonald's Blood Flow in Arteries*. Edward Arnold, London, fourth edition, 1998.

[40] *Fluent help*.

[41] R.M. Nerem. Vascular fluid mechanics, the arterial wall, and atherosclerosis. *Journal of Biomechanical Engineering*, 114:274–282, 1992.

[42] R.M. Nerem, M.J.A. Rumberger, D.R. Gross, R.L. Hamlin, and G.L.Geiger. Hot-film anemometry velocity measurements of arterial blood flow in horses. *Circ. Res.*, 10:301–313, 1974.

[43] H. Falsetti, K.M. Kiser, G.P. Francis, and E.R. Belmore. Sequential velocity development in the ascending and descending aorta of the dog. *Circ. Res.*, 21:328–338, 1972.

[44] W.A. Seed and N.B. Wood. Velocity patterns in the aorta. *Cardiovasc. Res.*, 5:319–330, 1971.

[45] J.F. Douglas, J.M. Gasiorek, and J.A. Swaffield. *Fluid Mechanics*. Pearson Prentice Hall, 4th edition, 2001.